International Journal of Thermal Sciences 193 (2023) 108511

Contents lists available at ScienceDirect

International Journal of Thermal Sciences

journal homepage: www.elsevier.com/locate/ijts

Accuracy of 2D numerical models towards the prediction of the fire resistance on LSF partition walls

Paulo A.G. Piloto [a,*], Stephan Gomes [a], Leonardo Torres [b], Carlos Couto [b], Paulo Vila Real [b]

[a] LAETA-INEGI, Instituto Politécnico de Bragança, Portugal
[b] RISCO, Department of Civil Engineering, University of Aveiro, Portugal

ARTICLE INFO

Keywords:
Fire
LSF walls
Computational models
Finite volume method
Hybrid finite element method

ABSTRACT

Lightweight steel framing (LSF) walls are commonly used in modern buildings due to their high strength-to-weight ratio and readiness for installation. However, empty cavities within these walls can pose a fire risk if not properly addressed. In order to ensure the fire resistance and performance of LSF walls with empty cavities, various modelling techniques can be employed. Two-dimensional thermal models can also be used to simulate the behaviour of LSF walls with empty cavities in a fire scenario. These models can predict the spread of heat through the empty cavity, allowing designers to identify potential fire hazards and make adjustments to the design to mitigate those risks.

Three different computational solution methods were used to compare the fire performance of LSF walls with void cavities. Solution method 1 considers the air-structure interaction in the cavity region. Solution method 2 considers the existence of interface elements for the radiation heat transfer in the cavity region allowing the cavity temperature prediction. Solution method 3 considers the convection and radiation in the cavity region with a prescribed cavity temperature from experiments (hybrid). Solution methods 1 and 3 give a small root mean square error (RMSE), when compared with solution method 2. Solution method 3 gives a better approximation because can capture the main fire events during the fire, such as the cracks and fall off. Based on the parametric study, a new proposal is presented to predict the fire resistance by insulation, depending on the gypsum type and thickness.

1. Introduction

Several design techniques may be used to comply with fire requirements in LSF walls. One common design technique is to use fire-rated assemblies, which are tested and rated for their ability to withstand fire during a specific period of time. These assemblies can include mineral wool insulation in the cavity or as an alternative layer (out of the cavity region), gypsum board, and other fire-rated materials. By incorporating these materials into the design of the LSF wall, the empty cavity can be effectively void or filled to protect against the spread of heat and flames. Another technique is the use of fire barriers, which are designed to prevent the spread of fire by blocking the heat flow and flames. These barriers can be applied in the form of intumescent coatings, fire-resistant caulks, or other materials that expand when exposed to heat, creating a barrier that blocks the spread of fire. Thermal models can also be used to simulate the behaviour of LSF walls with empty cavities in the case of a fire scenario. These models can predict the spread of heat through the empty cavity, allowing designers to identify potential fire hazards and make adjustments to the design to mitigate those risks. Fire testing can also be conducted on LSF wall assemblies to check the fire performance of the design. These tests typically involve exposing the wall assembly to a standard fire and measuring its ability to maintain structural stability (R) integrity (E) and insulation (I). Fire testing can be conducted on full-scale LSF wall assemblies to check the fire performance of the design and typically involve exposing one side of the wall assembly to a standard fire. While the aforementioned design techniques can help to ensure the fire performance of LSF walls with empty cavities, several issues can arise when modelling the behaviour of fire in the cavity region of the LSF wall. One issue is the difficulty in accurately predicting the behaviour of fire within the cavity. The complex nature of fire and the interactions between heat, hot gases, and materials can make it challenging to model the spread of heat through the cavity with high precision. Moreover, the cavities in the wall might be exposed to different fire scenarios and thus have different fire safety

* Corresponding author.Campus Santa Apolónia, 5300-253, Bragança, Portugal.
E-mail address: ppiloto@ipb.pt (P.A.G. Piloto).

https://doi.org/10.1016/j.ijthermalsci.2023.108511
Received 25 March 2023; Received in revised form 18 June 2023; Accepted 20 June 2023
Available online 28 June 2023

requirements. For instance, a cavity in the wall located on the ground floor might have different requirements than the one located on the upper floors, or external walls might have different requirements when compared to internal walls. Computational models and simulations are used to validate the accuracy of numerical models developed to predict the fire performance of the wall in the buildings. These models should be validated against experimental data, either from standard testing or from real-fire scenarios. Subsequently, they can be used to predict the fire performance of buildings and to evaluate the safety and effectiveness of fire protection systems. The discrepancies between the results obtained from numerical models and experimental results are usually defined by errors, that might be caused by several factors, such as model simplifications and limitations, uncertainty in input data, and experimental deviations. To reduce the difference between numerical and experimental results, several mitigation techniques can be employed, such as: model validation, sensitivity analysis, uncertainty quantification, and a combination of different models. Previous research has been developed to evaluate the fire resistance of LSF walls with and without insulation materials in the cavity region, the effect of the LSF geometry, and the effectiveness of the external protection layers, among other fire design solution methods.

Several experimental investigations have been done to study the effect of the LSF geometry, the steel quality and the effect of the protection materials. Y. Sakumoto et al., in 2003 [1] presented experimental tests for partition walls and exterior walls, using different types and numbers of gypsum layers. Reinforced gypsum board with inorganic fibres usually improved the insulation fire resistance. The authors also noticed that attaching plywood increases the stiffness of the assembly and improves the fire resistance, even being a combustible material, but the fire resistance is mainly governed by the protection and integrity of the gypsum boards. Prakash Kolarkar in 2010 [2], presented an innovative composite insulation method, changing the traditional position of the insulation material. The insulation material was placed between two layers of gypsum. In order to improve the insulation fire resistance (I), this author also noticed a bigger plateau (temperature almost constant due to free water evaporation) when using external protection layers when compared to cavity insulated LSF walls. The absence of insulation material in cavity helped to uniform the temperature in the steel cross section in comparison to cavity insulated LSF wall, which usually develops larger gradients in the cross section, forcing Hot Flanges (HF) to expand more than Cold Flange (CF), causing out-of -plane deformation towards the fire side. This author also presented an analytical method to foresee the ability to sustain the load under fire (R), based on the temperature evolution of the HF, using the correlation between the HF critical temperature and the load. Lázaro et al., in 2016 [3] made the thermal characterization of two different types of gypsum and developed their effective properties. These authors made four full scale experimental tests on partition walls and cladding walls, using both gypsum types, with the purpose to validate the FDS one dimensional numerical model. Ariyanayagam and Mahendran in 2017 [4] developed experimental fire tests on LSF partition walls with void cavities using gypsum boards to compare the fire insulation performance of calcium silicate and gypsum. These authors concluded that the fire performance was similar for both materials, but both materials gave higher fire resistance when compared to previously tested magnesium oxide boards. Calcium Silicate boards stayed intact during the fire tests and the gypsum boards did not, presenting cracks and falling off of parts. More recently, in 2019, Dias et al. [5,6] made experimental tests on LSF walls using steel sheeting, with and without load. This element (steel plate) is responsible to increase the mechanical stiffness and resistance at room and elevated temperature, but caused only marginal improvements in the LSF wall fire resistance, due to opening joints of steel and gypsum layers. Authors also used web stiffened studs that can bear 57% higher axial load in comparison to lipped studs. The steel sheeting increased the fire performance of gypsum boards due to the moisture confinement within this material and increased, significantly, the insulation fire resistance of LSF walls. In 2020, Magaraboosham et al. [7] made experimental tests to evaluate the effect of cavity depth for non-load bearing LSF walls, and verified that the temperatures on the unexposed side decrease with the thickness of the wall, contributing to improving the fire resistance. All experimental tests were made with void cavities, using single stud and double stud wall. Tao et al. [8] tested the effect of aerogel blanket, when used as an additional layer in contact with gypsum board for the fire protection of the LSF wall. This aerogel blanket improved the fire resistance, due to the reduction of the LSF temperature. The main disadvantage of this material is the overheating of the most exposed gypsum layers and the consequent failure of these plates. Fire tests were developed in Square Hollow Sections (SHS). Gnanachelvam et al. [9] tested the effect of the position and type of insulation materials towards the insulation fire resistance on LSF walls. These authors also concluded that the best position for the insulation material is not in the cavity region, but instead should be applied as an external composite protection layer in parallel to gypsum layers. Higher Hot Flange (HF) temperature is also expected when using the insulation material in the cavity region. These authors also tested phase-changed material (PCM) in combination with cellulose fibre, as insulation material, and verified an increase in the insulation fire resistance. The insulation material combination is also recommended to be used externally as a composite layer solution to enhance the fire resistance and the energy efficiency at room temperature.

Numerical investigations have been used to validate the models and avoid expensive testing conditions. These simulations are also used for parametric analyses in order to find the effect of design parameters. In 1996, Mohamed Sultan [10] presented the results obtained by the one-dimensional finite difference method developed to solve the heat transfer model and compared them with experimental results over time. The model considers convection and radiation from both gypsum layers facing the cavity region, but neglected the heat by radiation from the steel studs to the gypsum surface. According to this author, the effect of the steel stud on the heat transfer through the gypsum layers can be considered insignificant. This omission may justify the difference between experimental results and model predictions. This model presents conservative fire ratings when compared to the experimental results. This paper also presents the thermophysical properties of gypsum type X (herein identified as Gypsum 2). Geoff Thomas [11] in 2002, studied the effect of the thermal properties on gypsum plasterboard at elevated temperatures and developed a finite element thermal model for LTF walls. The thermal properties were adjusted to mimic physical events, such as ablation and cracks, and were modified to avoid numerical instabilities. The model was conservative and less accurate when compared with experimental measurements. The thermal properties were considered effective ones, and assumed to be suitable to use in the finite element models. C. Ang and Y. Wang in 2004 [12] investigated the effect of moisture movement in the gypsum layers, based on heat and mass transfer. The authors decided to use an equivalent (effective) specific heat, higher than the latent heat of water evaporation to skip the mass analysis and use only in the thermal analysis, without considering explicitly the moisture movement. Keerthan P. and Mahendran M. in 2012 [13] studied the fire performance of multiple layers of gypsum boards (without modelling the LSF system) using the SAFIR software and some previous experimental tests to validate the results. This study was developed in reduced-scale specimens to test the thermal performance under fire using different thermal properties of gypsum. This investigation highlights the risk of stepover the evaporation process from the gypsum material. To reduce this risk, these authors used a material property defined by the enthalpy equation. SAFIR is also using apparent thermal properties and is not able to model ablation. New simplified equations were proposed to predict the temperature evolution on the unexposed side of the gypsum layers when using varying thicknesses. This investigation also studied the effect of a 16 mm void cavity between two gypsum plates (13 mm), assuming the heat flow only by radiation between both gypsum plates, and concluded that the effect of

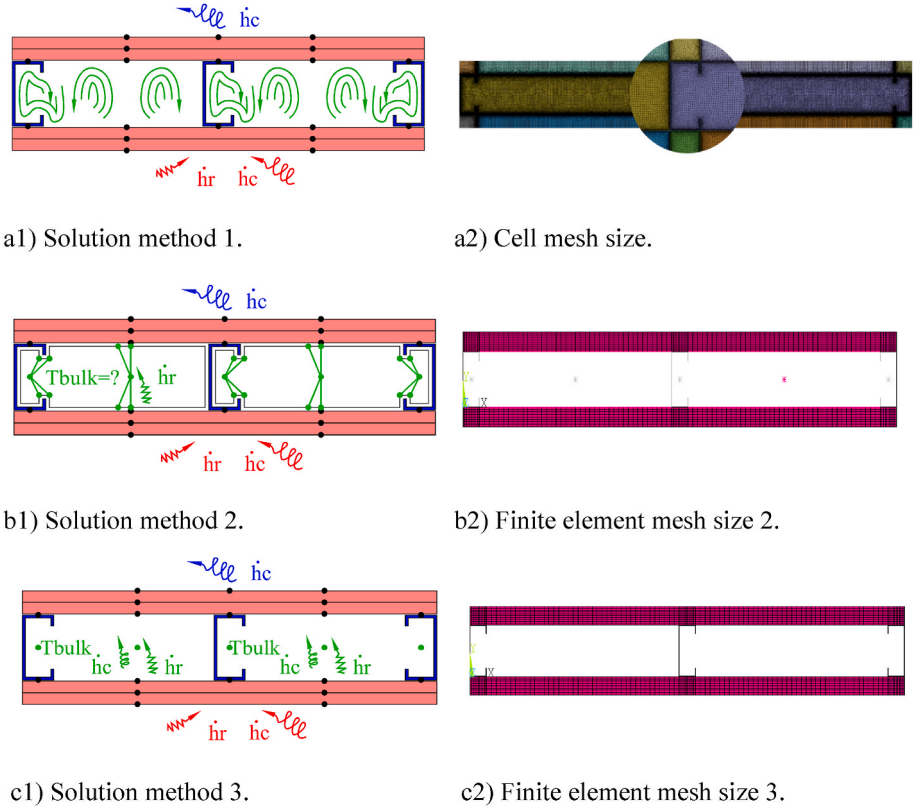

Fig. 1. Solution methods used to simulate the heat transfer in the cavity region.

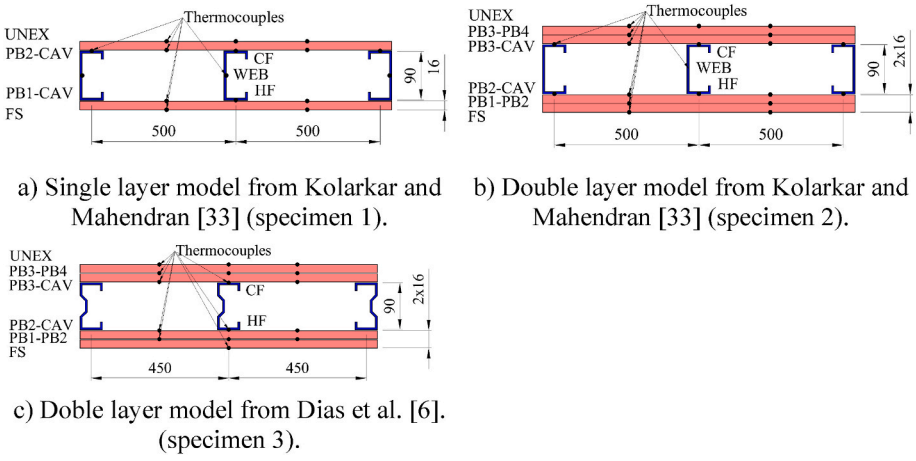

Fig. 2. Models selected for validation.

Table 1
Mesh size used for numerical validation.

	Solution method 1	Solution method 1	Solution time [s]	Solution method 2	Solution method 2	Solution time [s]	Solution method 3	Solution method 3	Solution time [s]
	Nodes	cells		Nodes	Elements		Nodes	element	
Specimen									
1	143491	135200	13231	2277	2308	32	2277	1888	58
2	155797	147303	15942	3620	3950	38	3620	3228	24
3	145025	136767	15465	3051	3084	47	3051	2288	44

the cavity could be negligible when compared with the solution of both gypsum plates without the cavity region. Ignoring the heat flow by convection will rise the temperature of the less exposed gypsum boards facing the cavity. Keerthan and Mahendran in 2013 [14] simulated the composite panels using SAFIR. These authors discussed the necessity to use apparent thermal properties, especially in the case of software not

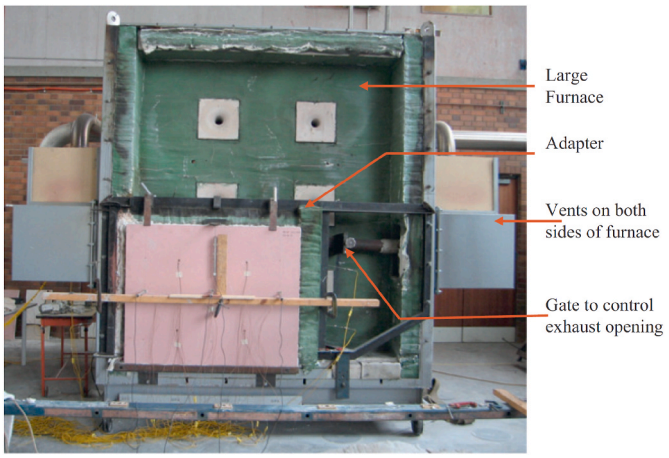

Fig. 3. Setup for test specimens 1 and 2, by Kolarkar and Mahendran [33].

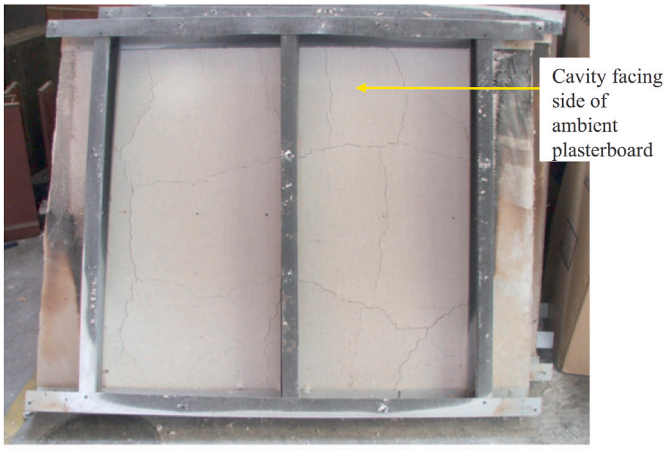

Fig. 4. Specimen 1 after the fire test, by Kolarkar and Mahendran [33].

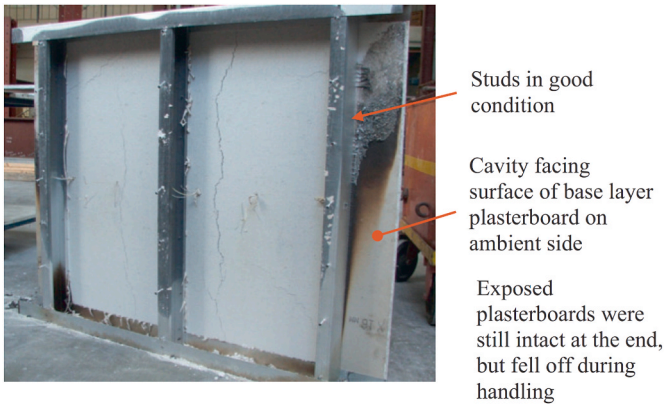

Fig. 5. Specimen 2 after the fire test, by Kolarkar and Mahendran [33].

running with the possibility to kill elements for ablation or to consider the moisture movement inside the gypsum layers. These authors identified again the risk to stepover the evaporation process during the simulation, when not ujsing the enthalpy thermal property. Gunalan and Mahendran, in 2013 [15] developed experimental tests and numerical studies with load to prove that filling the cavity region with insulation material will reduce the fire resistance (load bearing). Alternatively, using composite layers with insulation material in between gypsum

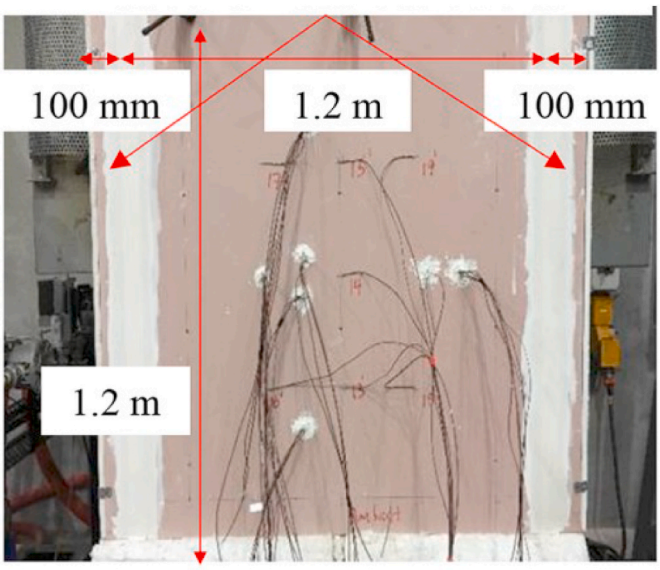

Fig. 6. Setup for test specimen 3, by Dias et al. [6].

Fig. 7. Gypsum board PB3 facing the cavity region, by Dias et al. [6].

plates, assuming void cavity, enhanced the insulation and load bearing performance of LSF walls. These authors used finite element software to simulate the structural performance of the LSF walls, using temperature evolutions from experiments. The model was able to predict the fire resistance within 5 min tolerance. These authors did not made any thermal analysis, instead they simplified the non-uniform temperature distribution, using linear and multi linear temperature across the web of the stud, based on temperature measurements. Rusthi et al., in 2015 [16] used the 3D finite element model, applying only radiation inside the cavity region. The gypsum thermal properties were considered as effective, being part of them, for some temperature levels, determined from experimental measurements. The ABAQUS 3D thermal model was validated with experiments developed in 2010, but no error information

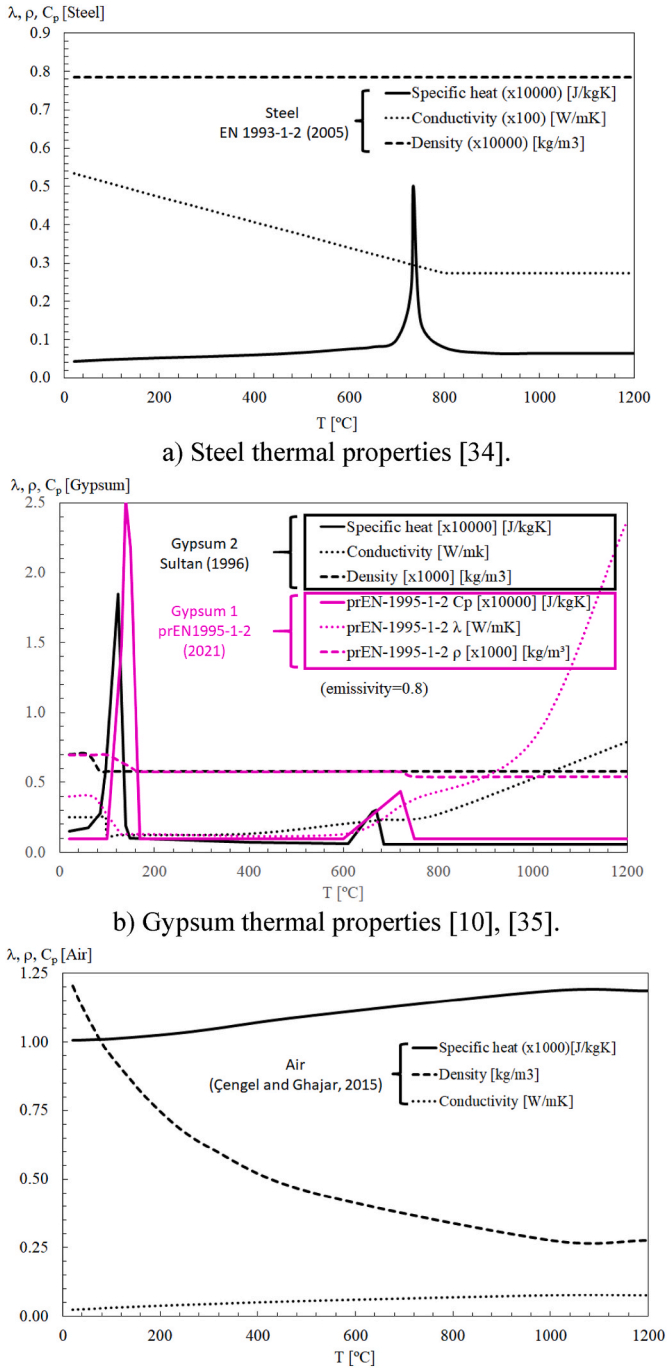

Fig. 8. Materials used for validation.

has been provided. These authors also developed numerical simulation with other cladding systems, such as magnesium oxide board, cement fibre board and perlite board. Jonathan Vallée in 2016 [17] developed ABAQUS 3D thermal models using radiation and conduction in the cavity region. The author compared only the fire resistance, using the relative error and found differences between the numerical and experimental results, ranging from 6% to 28%. This study did not compare the results over time. Authors also analysed the impact of small holes in the exposed surface and concluded that fire resistance may deacresed by 20% when the hole diameter increased 5 times. Lázaro et al. [3] in 2016, devloped also a numerical model based on FDS and the model was prepared to predict the ablation of the gypsum board at elevated temperatures. This event was identified by one temperature criterion (360 °C) applied to the back of the gypsum boards, and applied it by removing an equivalent mass of gypsum from the simulation. The heat transfer through the gypsum pores was modelled by convection and radiation. No information is given about the heat taranfer in the void cavity. The model was validated for the insulation fire reistance and for the temperature evolution during the fire tests. Tao et al. [8] in 2021 also made numerical simulations using ANSYS to validate the tests developed in SHS. Big adjustments were made to the thermal conductivity to include the potential ablation on gypsum and aerogel layers. These authors used 3D finite element models, based on shell and solid finite elements. The model used thermal radiation inside the hollow section with temperature dependent emissivity used for the steel hollow section and constant emissivities for the cavity regions. This different behaviour is not explained by the authors. The thermal effect of the screws was also neglected, but this is usually a very small sink effect. According to the authors, some adjustments were made to ensure that the modelling results could best fit the experimental results. Gypsum was modelled with "one reaction only" or two consecutive temperature-overlapped dehydration processes (free water evaporation) that usually occurs between 80 °C and 250 °C, and thermal conductivity was highly modified at elevated temperatures (ablation). These authors also found similar temperature evolution for the same LSF wall configuration, when testing reduced scale and full scale specimens. Tao et al. [18], in 2021, performed the validation of numerical models using LSF walls made with closed-formed steel hollow studs, highlighting the advantage of using these cross-section types without insulation material in the cavity, and using the insulation material in a composite external solution. The thermal simulation was developed using ANSYS and the heat transfer in the cavity region was made by radiation only, using constant emissivity for radiation in the cavity region and assuming temperature dependent emissivity for the hollow cross sections. The effects of localised plasterboard fall-off were not included in the simulation due to its unpredictability. The numerical results were in reasonable agreement with the experimental results. Special modelling techniques were tested to explore the effects of localised gypsum fall-off on the wall, using well defined square areas to evaluate the hot spot effect in the fire performance. Samiee et al. [19], in 2022, made a 3D numerical investigation using ABAQUS to investigate the effect of the steel sheathing and its position and the effect of gypsum strips near the studs. The thermal analysis in the cavity region accounted only for radiation and the authors neglected convection due to the very limited airflow inside the wall cavity. The steel plate did not modify the stud hot flange (HF) temperature, but the internal use reduced the cold flange (CF) temperature. This position is responsible for the increase of the temperature gradient over the stud cross-section. The authors also noticed that increasing the stud web depth decreases the temperature on the unexposed side, leading to an increase in the insulation fire resistance (I). The extra gypsum strips have a positive effect, acting as extra thermal insulation to the stud temperature, becoming very useful when superposed to the joints of gypsum plates. The use of gypsum strips can prevent a sudden increase in the temperature of the hot flange of the studs. The modelling of the cavity region was developed with radiation heat transfer only. Upasiri et al. [20] in 2022, made 2D and 3D numerical simulations using ABAQUS to test concrete based insulation materials placed in the cavity region, comparing autoclaved aerated concrete and concrete foam. Similar temperature evolution was determined at the center plane of the wall. The numerical results were compared with standard LSF walls without and with cavity insulation materials (rock wool), for different standard fire scenarios. The fire resistance (I) increased with the cavity filled with rock wool, and even more with concrete foam, for both fire scenarios (standard and hydrocarbon). The simulation of the cavity region was developed by radiation only, because, according to the authors, radiation dominates over conduction and convection. Higher convection coefficient was applied in the unexposed surface when compared to EN1991-1-2 [21], when using

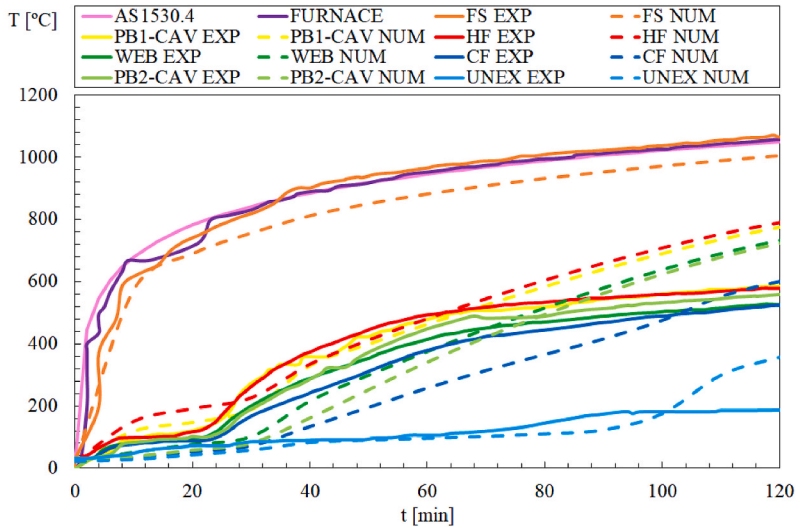

a) Specimen 1 with solution method 1.

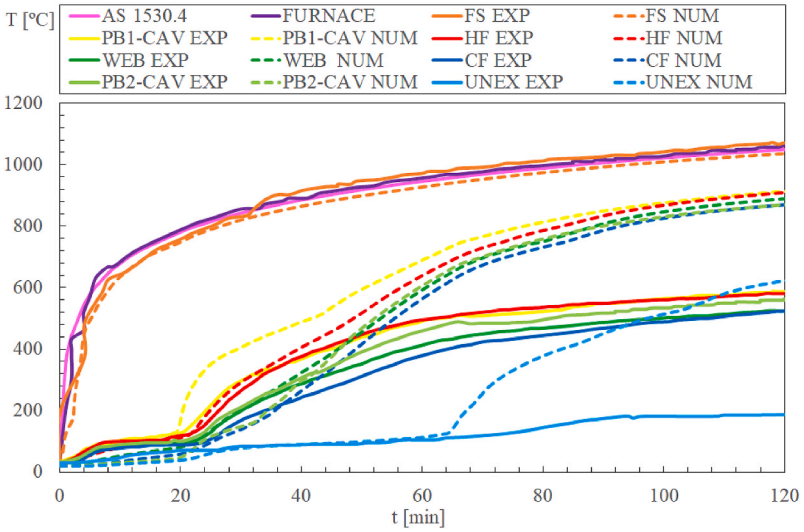

b) Specimen 1 with solution method 2.

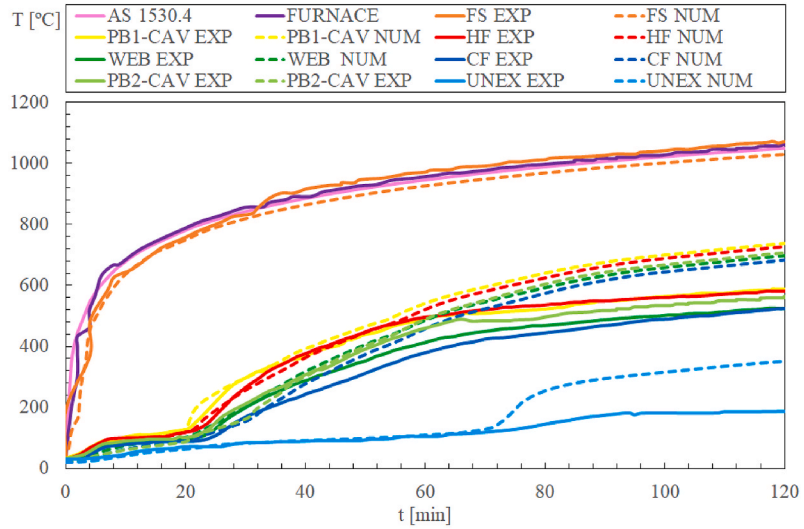

c) Specimen 1 with solution method 3.

Fig. 9. Comparison of results for specimen 1.

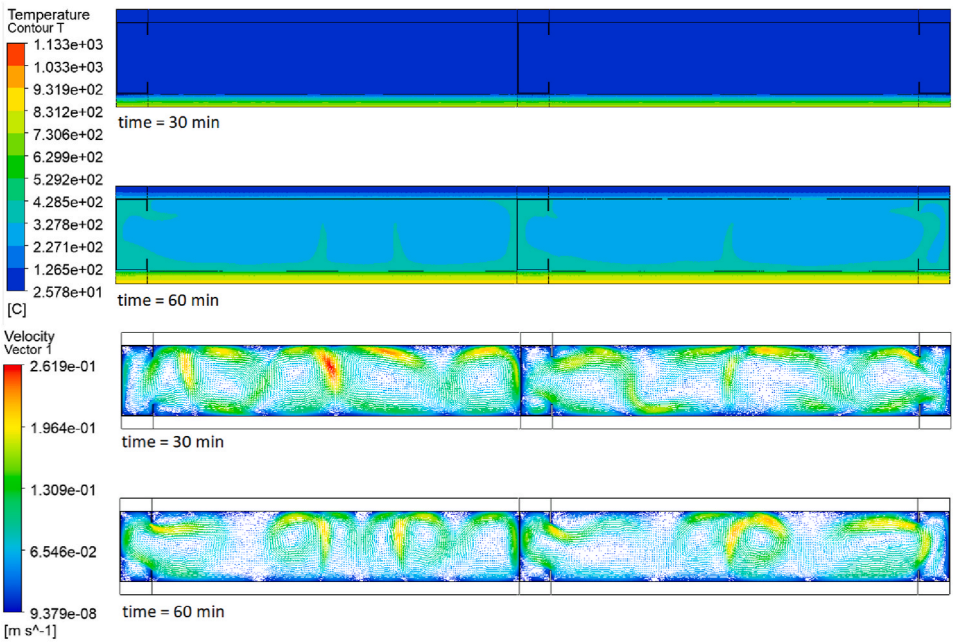

a) Specimen 1 with solution method 1.

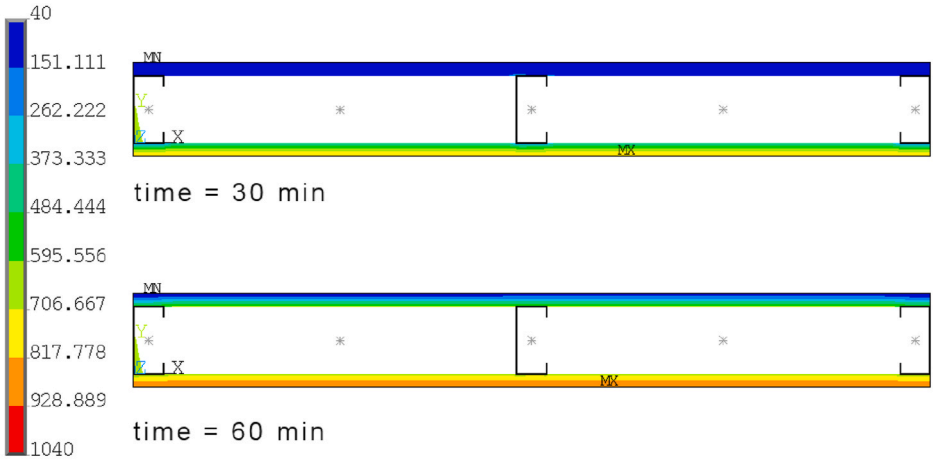

b) Specimen 1 with solution method 2.

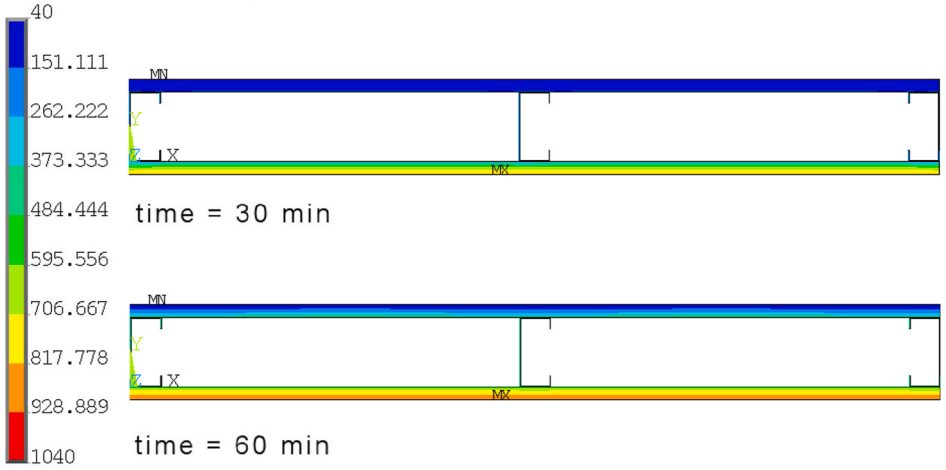

c) Specimen 1 with solution method 3.

Fig. 10. Temperature field from specimen 1 determined for each solution method.

Table 2
RMSE for the validation of specimen 1 (solution method 1).

Time steps	Time intervals	FS [°C]	Pb1 CAV [°C]	HF [°C]	WEB [°C]	CF [°C]	Pb2-CAV [°C]	UNEX [°C]	Average [°C]
6	0–60 min	86.7	52.3	44.6	59.6	95.5	112.4	18.3	67.1
10	0–100 min	82.4	66.2	72.3	70.2	87.8	94.8	26.0	71.4
12	0–120 min	79.9	93.2	104.9	102.8	84.7	105.0	63.6	90.6
									76.3

Table 3
RMSE for the validation of specimen 1 (solution method 2).

Time steps	Time intervals	FS [°C]	PB1-CAV [°C]	HF [°C]	WEB [°C]	CF [°C]	Pb2-CAV [°C]	UNEX [°C]	Average [°C]
6	0–60 min	33.8	123.0	68.2	86.1	90.1	79.0	16.6	71.0
10	0–100 min	34.1	206.5	176.6	201.1	201.7	179.8	161.5	165.9
12	0–120 min	33.9	229.9	208.9	235.3	231.8	206.3	224.6	195.8
									144.2

Table 4
RMSE for the validation of specimen 1 (solution method 3).

Time steps	Time intervals	FS [°C]	PB1-CAV [°C]	HF [°C]	WEB [°C]	CF [°C]	PB2-CAV [°C]	UNEX [°C]	Average [°C]
6	0–60 min	35.6	25.4	13.0	38.6	44.4	26.1	5.1	26.9
10	0–100 min	38.3	77.3	64.9	88.7	92.5	73.5	67.6	71.8
12	0–120 min	38.8	92.8	82.9	106.4	106.5	88.5	89.5	86.5
									61.7

Table 5
Comparison of the insulation fire resistance for specimen 1 (numerical results).

	Solution method 1				Solution method 2				Solution method 3			
t_{fi} EXP [min]	T_{MAX} [min]	T_{AVE} [min]	t_{fi} NUM [min]	Rel. Diff. [%]	T_{MAX} [min]	T_{AVE} [min]	t_{fi} NUM [min]	Rel. Diff. [%]	T_{MAX} [min]	T_{AVE} [min]	t_{fi} NUM [min]	Rel. Diff. [%]
89	99	100	99	11	65	65	65	26	73	73	73	18

both heat transfer modes (radiation and convection). Perera et al. [22] in 2022, made a numerical investigation using ABAQUS, in order to improve the fire resistance of LSF walls. The use of gypsum blocking stripes in both stud flanges (HF and CF) and the use of discontinuous cavity insulation with rock wool (not touching the steel studs), improved the insulation fire resistance. The authors only used radiation for modelling the thermal behaviour of the cavity region, neglecting convection.

The fire effect on LSF walls is being investigated by the authors of this manuscript, in order to: develop accurate numerical models based on the thermal analysis with air-structure interaction [23]; compare the numerical with experimental results developed by other researchers [24], analyse the fire resistance of LSF using the simplified one-dimensional heat flow [25]; present a sequence of simulations to analyse the fire resistance of LSF walls made with composite panels [26], based on a hybrid finite element model [27,28]. Recently, a new research has been also established on double stud LSF walls [29] and on the analysis of the critical temperature on load bearing LSF walls [30]. The experimental tests have been developed using reduced and full-scale LSF wall specimens and the numerical simulations were developed accordingly.

This investigation compares three numerical simulation methods, and establishes the best computational modelling technique to simulate the fire behaviour in the cavity region. New insights into the physics of the process are presented, using the numerical validation with experimental tests. Authors also compared the effect of two different gypsum materials and stud geometries.

2. Methods, models and materials

Three different two-dimensional (2D) solution models are represented to simulate the fire performance of the non-load-bearing LSF wall. These models assume perfect contact between materials, see Fig. 1. This assumption is being used by other researchers and looks to be a reasonable approximation due to the construction process. The cladding system is usually tied to the LSF structure using self-drilling screws. The current generation of LSF structures is machined and recessed to assume that gypsum plasterboards are perfectly flat with no singular effect of overlapping studs and tracks.

Solution method 1 uses the finite volume method (FVM) with thermal and fluid interaction for the solid and fluid parts. This method assumes laminar flow and is based on density variation. The fluid motion is induced by heat transfer, and the solution is transient and nonlinear. The density-based solver considers the equations of continuity, momentum, energy, and solve them simultaneously, using Ansys Fluent [31]. Pressure is obtained through the equation of state. Governing equations for additional scalars are solved afterwards and sequentially (radiation). The integration time for each time step was 60 s, with the possibility to be reduced to 1 s. The convergence criterion was based on the residuals for each equation. In the numerical model, the cross-section is divided into finite cells where the domain variables, i.e., pressure, velocity and temperature are calculated, at the same time. The grid for all the domains (solid and fluid) is presented in Fig. 1, using the minimum cell size equal to 0.0003 m.

Solution method 2 uses the finite element method (FEM) and considers only the thermal analysis for solids, assuming perfect contact

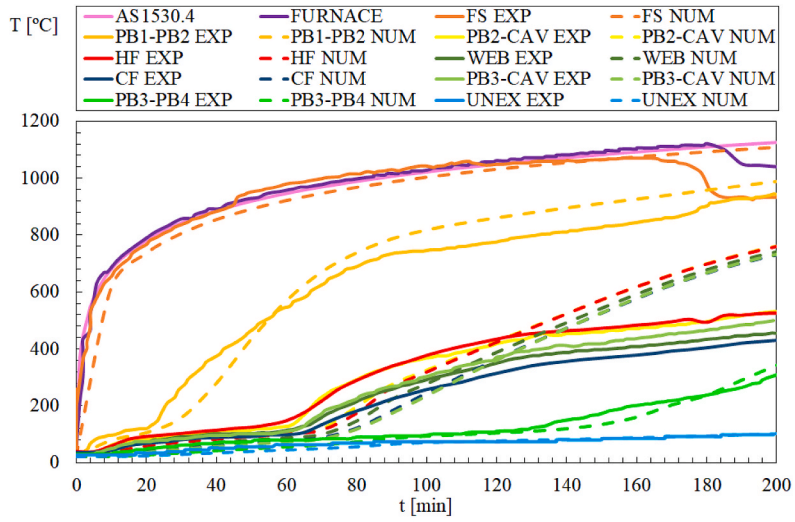

a) Specimen 2 with solution method 1.

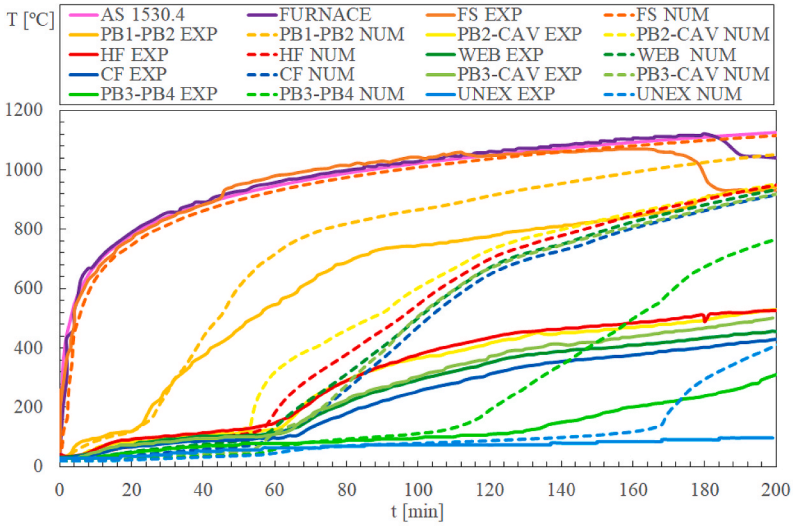

b) Specimen 2 with solution method 2.

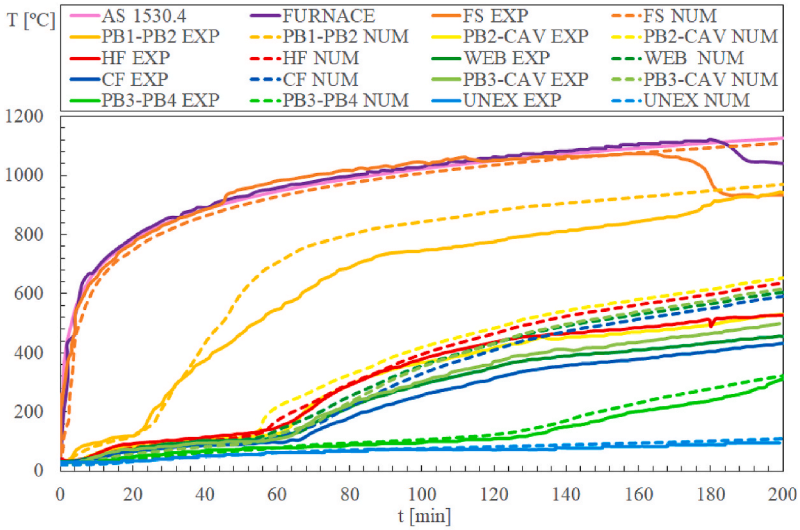

c) Specimen 2 with solution method 3.

Fig. 11. Comparison of results for specimen 2.

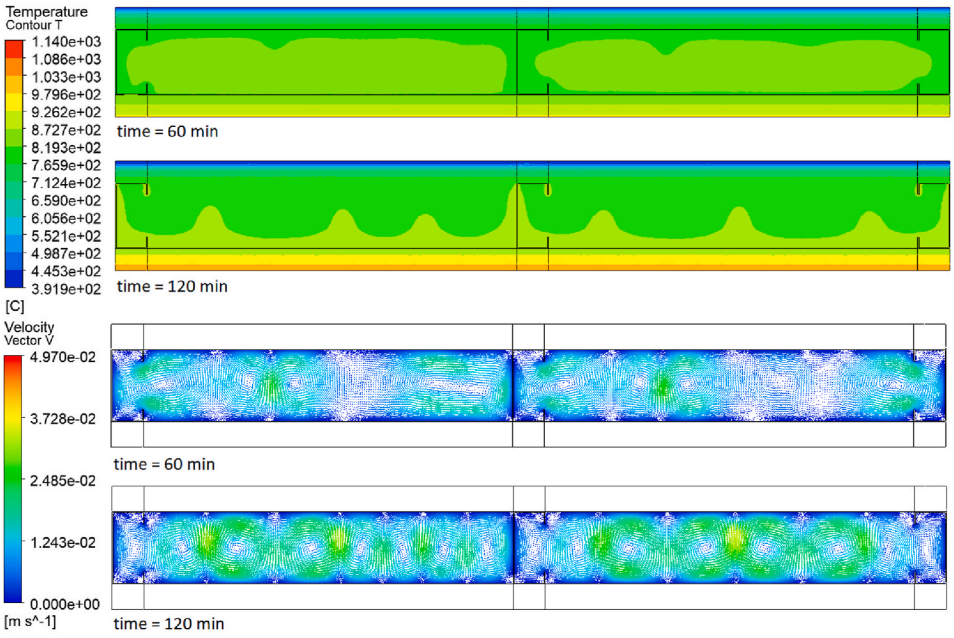

a) Specimen 2 with solution method 1.

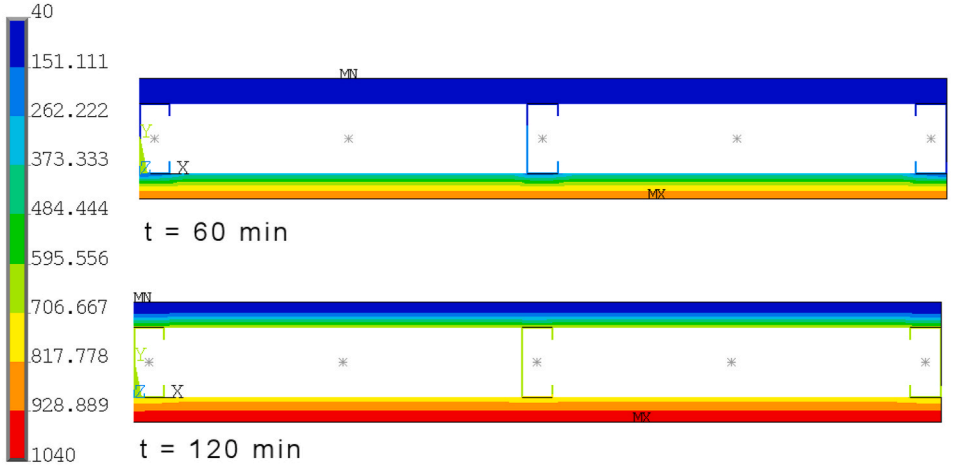

b) Specimen 2 with solution method 2.

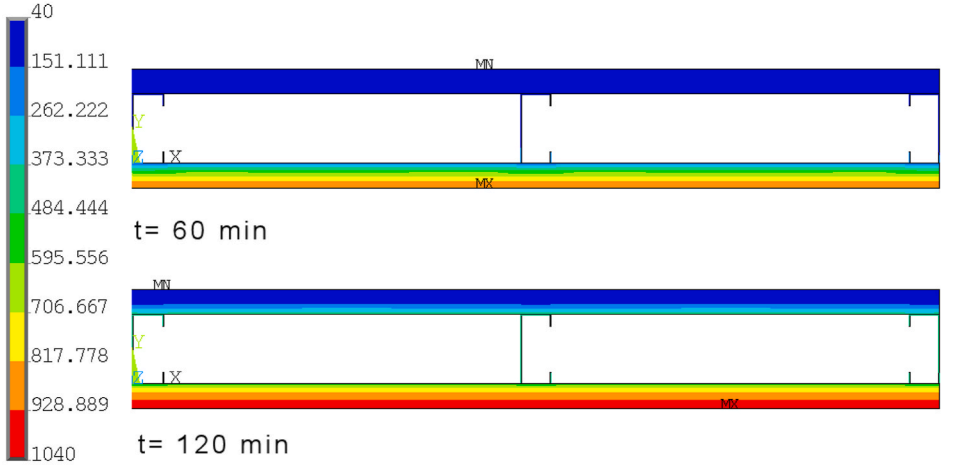

c) Specimen 2 with solution method 3.

Fig. 12. Temperature field from specimen 2 determined for each solution method.

Table 6
RMSE for the validation of specimen 2 using the solution method 1.

Time steps	Time intervals	FS [°C]	Pb1–Pb2 [°C]	Pb2 CAV [°C]	HF [°C]	WEB [°C]	CF [°C]	Pb3 CAV [°C]	Pb3–Pb4 [°C]	UNEX [°C]	Average [°C]
6	0–60 min	46.8	67.0	22.5	34.6	27.7	24.9	36.7	25.0	14.8	33.3
10	0–100 min	47.1	61.2	56.5	63.9	40.1	33.5	64.6	21.6	13.5	44.7
12	0–120 min	49.2	66.5	56.6	65.0	40.2	34.2	66.0	21.7	13.5	45.9
											41.3
14	0–140 min	41.8	68.2	52.1	57.5	48.0	49.5	58.4	23.1	11.5	45.6
18	0–180 min	45.5	70.2	90.3	89.3	103.4	111.0	90.5	25.3	10.2	70.6
											48.0
20	0–200 min	69.2	68.2	110.8	110.4	131.4	139.9	111.3	25.5	9.7	86.3
											54.4

Table 7
RMSE for the validation of specimen 2 using the solution method 2.

Time steps	Time intervals	FS [°C]	Pb1–Pb2 [°C]	Pb2-CAV [°C]	HF [°C]	WEB [°C]	CF [°C]	Pb3-CAV [°C]	Pb3–Pb4 [°C]	UNEX [°C]	Average [°C]
6	0–60 min	34.5	93.6	78.0	22.3	21.6	24.4	41.2	27.5	15.1	39.8
10	0–100 min	36.7	110.6	134.1	77.4	89.4	87.8	82.4	21.9	11.8	72.5
12	0–120 min	35.1	114.8	172.0	121.8	145.5	149.9	135.7	31.6	12.0	102.0
											71.4
14	0–140 min	32.6	119.2	203.9	160.3	188.7	195.5	176.0	70.7	13.4	128.9
18	0–180 min	40.7	125.2	257.8	225.4	259.0	266.8	237.4	173.2	54.8	182.3
											105.1
20	0–200 min	68.6	124.0	278.2	250.9	287.0	294.9	260.6	218.8	104.8	209.8
											122.5

Table 8
RMSE for the validation of specimen 2 using the solution method 3.

Time steps	Time intervals	FS [°C]	Pb1–Pb2 [°C]	Pb2-CAV [°C]	HF [°C]	WEB [°C]	CF [°C]	Pb3-CAV [°C]	Pb3–Pb4 [°C]	UNEX [°C]	Average [°C]
6	0–60 min	34.6	88.9	36.1	13.7	9.6	9.3	13.2	6.8	3.0	23.9
10	0–100 min	37.3	99.4	38.1	12.7	28.9	31.7	21.2	6.5	3.2	31.0
12	0–120 min	35.9	100.1	43.4	15.5	40.5	47.0	30.4	7.9	4.5	36.1
											30.4
14	0–140 min	33.4	99.9	50.7	23.9	51.7	60.2	41.3	10.6	5.9	41.9
18	0–180 min	40.1	95.4	69.1	44.8	73.2	83.3	61.2	18.8	6.8	54.7
											37.5
20	0–200 min	66.6	91.0	75.8	53.8	83.1	93.2	68.7	68.7	7.4	67.6
											42.6

Table 9
Comparison of the fire resistance for specimen 2 (NA= Not Applicable).

	Solution method 1				Solution method 2				Solution method 3			
t_{fi} EXP [min]	T_{MAX} [min]	T_{AVE} [min]	t_{fi} NUM [min]	Rel. Diff. [%]	T_{MAX} [min]	T_{AVE} [min]	t_{fi} NUM [min]	Rel. Diff. [%]	T_{MAX} [min]	T_{AVE} [min]	t_{fi} NUM [min]	Rel. Diff. [%]
>200	241	240	240	NA	169	168	168	NA	>200	>200	>200	NA

between materials. The transient and nonlinear thermal analysis is solved, with full-option solution method. The energy equation is solved by the weighted residual method and the Galerkine method, with the application of the weak integral formulation. The same time step has been used with a similar convergence criterion for the heat flow. Fig. 1 represents the finit element mesh. One additional boundary condition is applied in the cavity region, assuming heat transfer by radiation between all the internal faces. This model can predict the cavity temperature of the cavity region, just by performing the thermal equilibrium of the internal faces of this region. The two-dimensional (2D) analyses were made using the finite element PLANE55 and SURF151, both available in the Ansys APDL [32]. The PLANE55 element is defined by four nodes with a single degree of freedom (temperature), uses linear interpolating functions and a full gauss integration scheme (2 × 2) to define the conductivity matrix. The SURF151 finite element is overlaid onto the edge of the PLANE55 finite element, either representing an interface element with gypsum or representing an interface element with steel, to define the heat flow by radiation between this edge surface and the nodal cavity temperature of the cavity. This element is defined by three nodes, being two nodes coincident with the region in contact with the cavity and the third node to define the cavity temperature evolution, the latter being placed at the geometric centre of the cavity

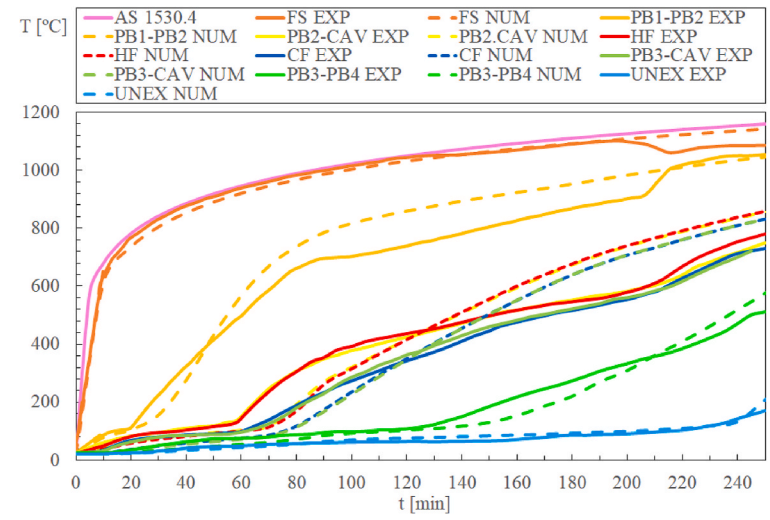

a) Specimen 3 with solution method 1.

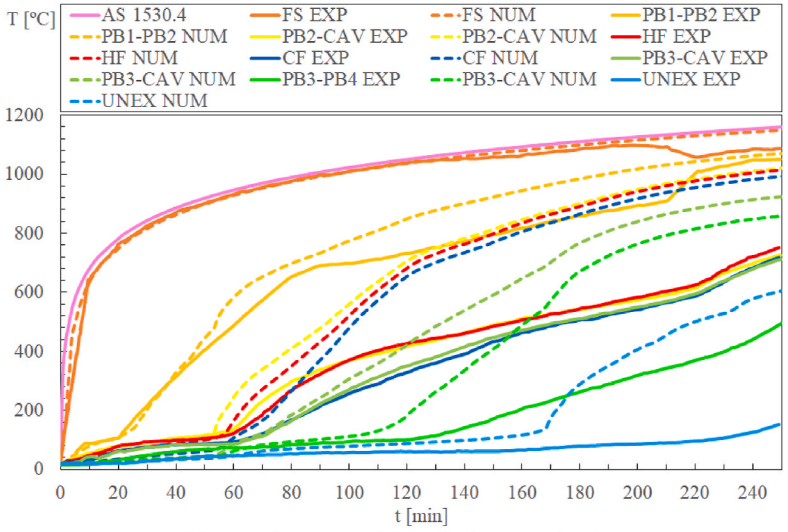

b) Specimen 3 with solution method 2.

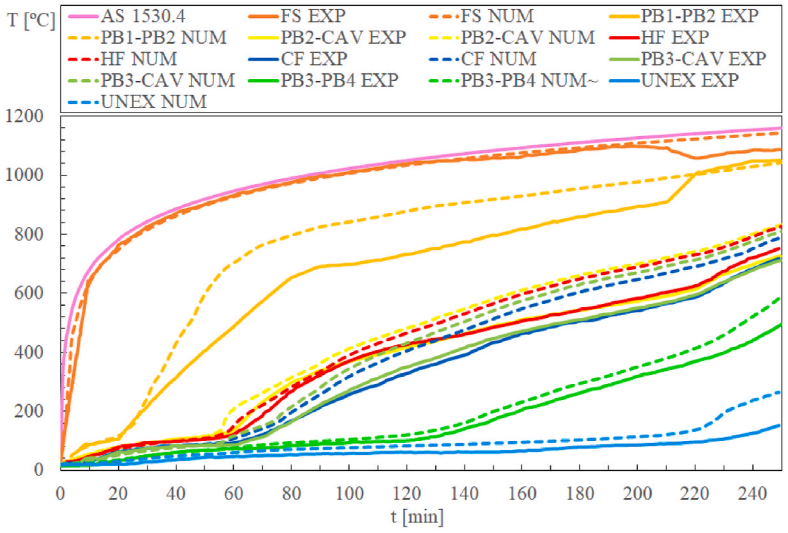

c) Specimen 3 with solution method 3.

Fig. 13. Comparison of results for specimen 3.

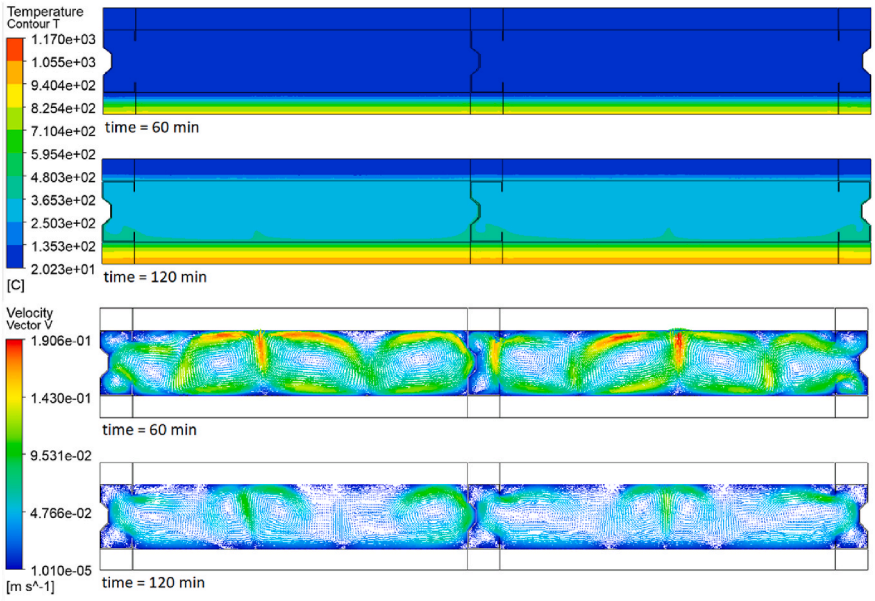

a) Specimen 3 with solution method 1.

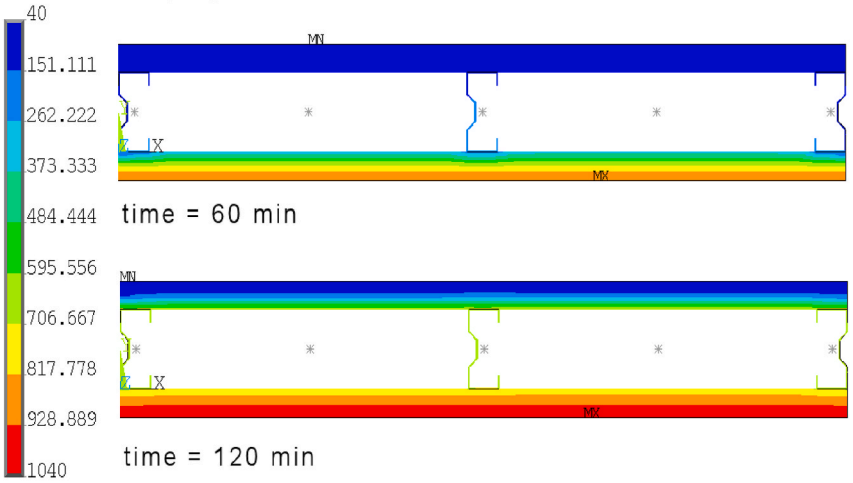

b) Specimen 3 with solution method 2.

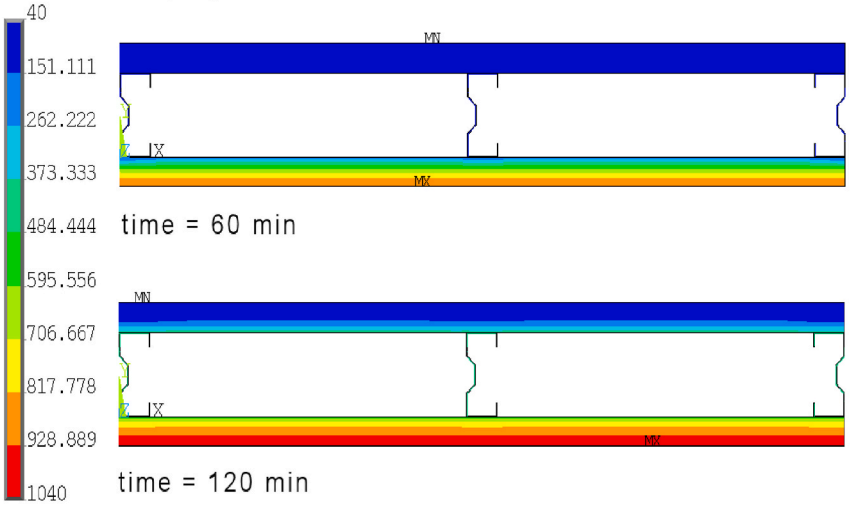

c) Specimen 3 with solution method 3.

Fig. 14. Temperature field from specimen 3 determined for each solution method.

Table 10
RMSE for the validation of specimen 3 using the solution method 1.

Time steps	Time intervals	FS [°C]	Pb1–Pb2 [°C]	Pb2-CAV [°C]	HF [°C]	WEB [°C]	CF [°C]	Pb3-CAV [°C]	Pb3–Pb4 [°C]	UNEX [°C]	Average [°C]
6	0–60 min	23.6	45.5	27.5	27.7		26.1	26.5	19.3	6.4	25.3
10	0–100 min	20.5	67.4	66.5	73.0		41.4	42.5	17.6	6.1	41.9
12	0–120 min	19.5	78.4	61.5	68.7		38.1	40.7	16.3	6.9	41.3
											36.2
14	0–140 min	18.2	84.3	57.9	64.3		38.2	38.3	18.0	8.6	41.0
18	0–180 min	15.3	81.9	63.6	69.3		52.2	50.3	30.4	9.1	46.5
											39.2
20	0–200 min	15.4	85.8	78.8	85.0		69.9	67.6	32.0	9.4	55.5
											41.9

Table 11
RMSE for the validation of specimen 3 using the solution method 2.

Time steps	Time intervals	FS [°C]	Pb1–Pb2 [°C]	Pb2-CAV [°C]	HF [°C]	WEB [°C]	CF [°C]	Pb3-CAV [°C]	Pb3–Pb4 [°C]	UNEX [°C]	Average [°C]
6	0–60 min	7.9	43.3	44.1	20.2		25.0	34.6	17.7	3.4	24.5
10	0–100 min	6.4	52.6	96.5	71.9		93.4	30.5	15.4	11.7	47.3
12	0–120 min	5.8	65.2	140.6	115.3		150.5	37.1	28.4	14.9	69.7
											47.2
14	0–140 min	5.9	77.2	177.1	154.4		189.8	55.1	69.9	19.2	93.6
18	0–180 min	9.0	90.7	224.9	208.0		233.5	106.5	164.3	59.8	137.1
											74.4
20	0–200 min	10.0	94.8	243.8	227.4		250.7	135.3	208.8	109.4	160.0
											88.7

Table 12
RMSE for the validation of specimen 3 using the solution method 3.

Time steps	Time intervals	FS [°C]	Pb1–Pb2 [°C]	Pb2-CAV [°C]	HF [°C]	WEB [°C]	CF [°C]	Pb3-CAV [°C]	Pb3–Pb4 [°C]	UNEX [°C]	Average [°C]
6	0–60 min	7.9	127.2	28.9	12.1		7.4	14.4	3.4	10.4	26.5
10	0–100 min	6.5	139.1	29.8	17.1		26.2	36.8	5.9	14.3	34.5
12	0–120 min	6.1	140.4	36.8	20.8		38.9	46.4	8.3	15.8	39.2
											33.4
14	0–140 min	5.8	140.2	45.8	30.1		47.7	53.9	10.7	17.8	44.0
18	0–180 min	7.5	133.9	64.1	51.7		59.2	69.0	69.0	20.5	59.4
											40.7
20	0–200 min	7.9	130.0	72.6	59.7		65.2	75.6	18.1	21.3	56.3
											43.3

Table 13
Comparison of the fire resistance for specimen 3.

	Solution method 1				Solution method 2				Solution method 3			
t_{fi} EXP [min]	T_{MAX} [min]	T_{AVE} [min]	t_{fi} NUM [min]	Rel. Diff. [%]	T_{MAX} [min]	T_{AVE} [min]	t_{fi} NUM [min]	Rel. Diff. [%]	T_{MAX} [min]	T_{AVE} [min]	t_{fi} NUM [min]	Rel. Diff. [%]
252	247	244	244	3	170	169	169	33	226	225	225	10

region. The interpolating functions are also linear and the number of integration points is two.

Solution method 3 uses the hybrid finite element method (H-FEM) to simulate heat transfer by radiation and convection in the cavity region. This model can be used to determine the fire resistance of LSF wall with void cavities, based on the behaviour of the cavity temperature from previous experiments. The cavity temperature can be determined either by previous experimental measurements (plate thermocouples), or using the average temperature between the internal faces in contact with the cavity, of the most exposed layer (hot) and less exposed layer (cold), or using the average temperature of the Hot Flange (HF) and Cold Flange (CF). The main advantage of this hybrid solution method is that it considers any crucial event in the cavity region that affects the temperature evolution, namely the appearance of any crack, fall-off of boards, combustion of the materials, or any other heat release from the materials. This solution method requires the existence of radiation and convection inside the cavity region. The convection coefficient can be assumed to be 17 (W/m^2K), the average value between the value at fire exposed surface (25 W/m^2K) and fire unexposed surface, taking into account radiation (9 W/m^2K) coefficients. This assumption is physically admissible if one considers that the cavity region is initially protected at the start of the fire test and fully exposed to fire at the end of the test. The

Table 14
Fire resistance for the parametric study.

Specimen	Stud type/ Distance [mm]	Material/ Thickness [mm] Layer 1	Material/ Thickness [mm] Layer 2	t (Tmax) [min]	t (Tave) [min]
A	C/500	Gypsum 1/ 12.5		73	60
B	C/500	Gypsum 2/ 12.5		61	51
C	C/500	Gypsum 1/ 16.0		100	99
D	C/500	Gypsum 2/ 16.0		84	81
E	C/500	Gypsum 1/ 12.5	Gypsum 1/ 12.5	173	172
F	C/500	Gypsum 2/ 12.5	Gypsum 2/ 12.5	142	141
G	C/500	Gypsum 1/ 16.0	Gypsum 1/ 16.0	241	240
H	C/500	Gypsum 2/ 16.0	Gypsum 2/ 16.0	198	194
I	S/450	Gypsum 1/ 12.5		74	71
J	S/450	Gypsum 2/ 12.5		60	57
K	S/450	Gypsum 1/ 16.0		97	95
L	S/450	Gypsum 2/ 16.0		82	81
M	S/450	Gypsum 1/ 12.5	Gypsum 1/ 12.5	177	174
N	S/450	Gypsum 2/ 12.5	Gypsum 2/ 12.5	145	143
O	S/450	Gypsum 1/ 16.0	Gypsum 1/ 16.0	247	244
P	S/450	Gypsum 2/ 16.0	Gypsum 2/ 16.0	200	196

two-dimensional (2D) analyses were made using the finite element PLANE55 alone, imposing the cavity temperature in this region.

All these models were simulated with the traditional boundary conditions applied on the exposed side, i.e. convection with the convective coefficient of $\alpha_c = 25$ W/m^{2}K and radiation with the emissivity of the flames equal to $\varepsilon_f = 1$, and on the unexposed side (only convection with the convective coefficient of $\alpha_c = 9$ W/m^{2}K), [21].

The numerical validation is discussed in light of the prediction of the fire resistance and fire performance during the tests. Two distinct stud geometries have been selected, considering the experimental tests developed by Kolarkar and Mahendran [33], where the LSF walls are using three lipped studs type C 90 × 40 × 15x1.15 made of G500 steel grade, spaced every 500 mm, see Fig. 2, and the experimental tests developed by Dias et al. [6], where the LSF walls are using three web-stiffened studs type Σ, 90 × 40 × 15x1.15 made of G500 steel grade, spaced every 450 mm, see Fig. 2. Both structures were protected by multiple 16 mm thick fireproof gypsum boards (gypsum 1) in single or double layers. The position of the thermocouples is identified by small circles and identified according to their position, from fire side (FS) to the unexposed side (UNEX).

The mesh size depends on the solution methods and specimens. Table 1 presents the number of nodes and elements/cells used for each computational model. The computing time used for the solution is also included. One can see that solution method 1 has a computing time much slower when compared to the others.

The experimental tests developed by Kolarkar and Mahendran [33] were made in a vertical furnace running with propane gas burners, adjusting the dimension of the vertical furnace to the dimension of the specimen, see Fig. 3. The exposed surface of the LSF wall was submitted to standard fire AS1530.4, using the prescribed temperature curve. The furnace temperature (FURNACE) was controlled by the system, using the average of four thermocouples to compare with the prescribed temperature curve. The specimens were free to expand during each test. The insulation wool was used around the specimens to prevent heat loss for these regions.

Three type K thermocouples were positioned along the mid-height of each stud to measure the hot flange (HF), web (WEB), and cold flange (CF) temperatures. These temperatures were then averaged for each common position. Other thermocouples were positioned in contact with the gypsum plates to measure additional temperatures, such as the fire side on the exposed gypsum plate (FS), the gypsum temperatures facing the cavity region (PBi-CAV) or the interface temperatures between the overlapping gypsum boards (PBi-PBj). Five thermocouples were used in the unexposed surface (UNEX) positioned according to the standard.

According to the test observation of specimen 1 made by Kolarkar and Mahendran [33], the gypsum boards were damaged but they did not fall off, see Fig. 4. The cracks were randomly developed and no possible prediction is possible, due to the existence of geometric and material imperfections. One single gypsum board was responsible to keep the light steel frame temperature below 100 °C during 20 min.

Specimen 2 has been exposed to fire for 3 h. Experimental observations made after the test revealed that gypsum boards PB1 and PB2 were still positioned in place. The gypsum board PB3 facing the cavity on the unexposed side was also damaged with visible cracks, but presenting a different pattern from the previous one, see Fig. 5.

Specimen 3 was tested using a different setup, see Fig. 6. This furnace was running with a propane single burner, located at its centre. The LSF structure was protected by insltuation material around the edges, to minimize the heat flow in these directions. The tests has been developed until the insulation or integrity failure of the LSF wall.

The average temperature has been determined for every measuring zone. The fire side (FS) follows closely the standar fire curve until 210 min, when there was a sudden decrease coincindent with the sudden increase of the PB1-PB2 temperature. This event may be related with the falling off of the most exposed gypsum board. The integrity of the gypsum board PB3 can be observed in Fig. 7 and explains the uniform temperature development in the unexposed side [6], being the average temperature identified by (UNEX EXP).

The thermal properties from the materials were selected from established standards [34,35] and experimental studies [10,36], see Fig. 8. Two different types of gypsum plasterboard were used in this investigation. Gypsum 1 was used to validate the experimental tests. Both plasterboards (Gypsum 1 and Gypsum 2) were used to develop the parametric study, because they represent the most used thermal properties for the gypsum plates in Portugal. Since these properties are temperature dependent, to effectively solve the numerical models, an incremental and iterative method must be employed due to the nonlinearity of the solution. For the solution of the computational method 1, the iterative method is based on the verification of the residuals for velocity, using the absolute difference of 10^{-3} in each direction, the residual for the continuity with an absolute difference of 10^{-3}, and the residual for temperature with an absolute difference of 10^{-6}. For solution methods 2 and 3, the convergence is verified by the heat flow, using a tolerance value of 0.001 and a reference value of 10^{-6} [W].

3. Accuracy of the numerical models

This section presents the comparison of the results for each model, using the three solution methods. The comparison is presented by the Root Mean Square error (RMSE) for the temperature evolution of each component and by the relative error used to determine the fire resistance attained by insulation (I).

The steel frame from test specimen 1 was fire protected by a single layer of gypsum board (16 mm) [33]. The gypsum boards were connected to the studs by self-drilling screws at 300 mm centres for the studs and 250 mm centres for the tracks. Thermocouple type K were welded to the LSF profiles, three on each stud at mid-height to measure the

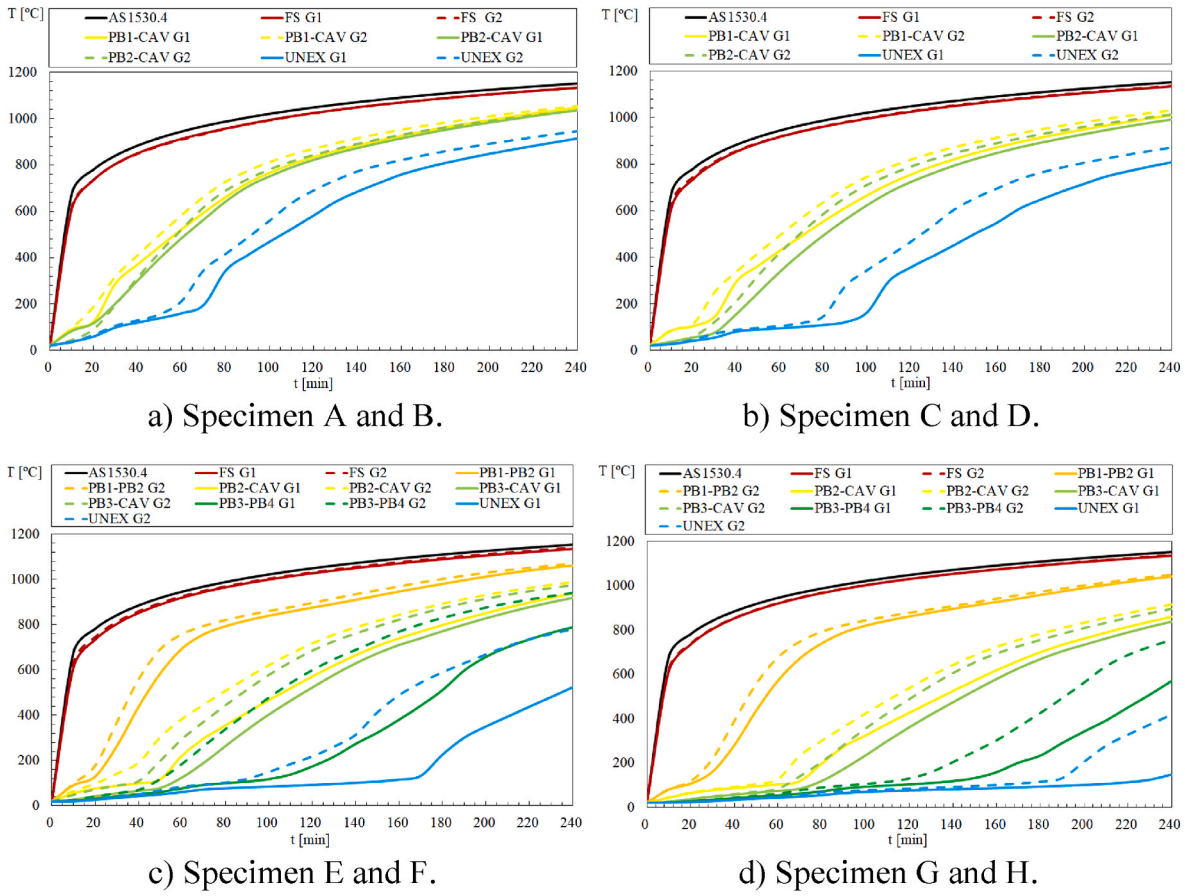

Fig. 15. Temperature evolution during fire exposure using stud type "C".

temperatures of the hot flange (HF), web (WEB), and the cold flange (CF). Additional thermocouples were attached to the gypsum boards to measure temperatures inside the wall cavity and on the fire exposed surface. External thermocouples have been placed on the unexposed surface to measure the ability to sustain the temperature on this side (UNEX), see Fig. 2. These temperatures are compared to the numerical results obtained for the same position, with the exception to the unexposed surface of the numerical model, where the Tmax and Tave have been determined by the average of 14 nodal temperatures.

Fig. 9 presents the comparison between the experimental (continuous lines) and the numerical results (dashed lines). Temperatures in each component have been compared for specimen 1. This specimen was tested under fire during 3 h. According to the authors, both the exposed and unexposed gypsum boards were severely affected, but did not fall off. The LSF was also in good condition [33]. The experimental unexposed temperature is represented by UNEX EXP and represents an average value. The temperature evolution at this location (UNEX EXP) presents an odd evolution showing a very large plateau, even with the increase of the furnace temperature between 89 and 120 min. For that reason, this comparison is only presented until this time window. According to Kolarkar and Mahendram [33], the insulation failure of this specimen occurred at 89 min. The most exposed single gypsum board of 16 mm provided an initial protection of about 20 min to the steel studs, with the stud temperatures increasing rapidly after this time. The average temperature (UNEX) is compared for all solution methods being noticed that this evolution starts to increase sooner when using solution method 2 after 65 min and later on when using solution method 1 (99 min). Solution method 2 presents higher temperature values for the steel components (HF, WEB, CF) when compared to the other solution methods, because it only considers the heat exchange by radiation in the cavity region. The temperature field is also depicted in the solid region for all solution methods, including the air temperature in the fluid region for solution method 1. It should be noted that the gravity acceleration was activated in the perpendicular direction to the gypsum plates to force the motion of the air due to temperature variation in this 2D model. The motion of the air particles may be detected by the vector velocity field, including the fluid regions inside the stud flange and lip. The maximum velocity decreases with the duration of the fire simulation because the difference between the temperature of the gypsum layers in contact with the cavity region decreases.

Fig. 10 depicts the temperature field from specimen 1 for all the solution methods, including the air velocity field for solution method 1. The results are presented for 30 min and 60 min after the start of the simulation.

The RMSE is small when using solution method 1 and solution method 3. The authors consider a good result for any RMSE determined in each component smaller than 100 °C, following the recommendation of the fire testing standard EN1363-1 [37]. This standard specifies that at any time after the first 10 min of the test, the temperature recorded by any thermocouple in the furnace shall not differ from the corresponding temperature of the standard fire curve by more than 100 °C. Solution method 2 is producing higher RMSE and this may be explained by the missing component for the heat flow (convection). This missing heat flow is responsible to raise the temperature in the cavity region, with higher discrepancies noted to the HF, WEB, CF and both temperatures of the gypsum plates in contact with the cavity region. Table 2, Table 3, and Table 4 present the RMSE determined for each solution method. For the first 60, 100 and 120 min of comparison. Solution method 1 presents an average RMSE of 76.3 °C, while solution method 2 is presenting an average RMSE of 144.2 °C. The RMSE for solution method 3 is 61.7 °C.

The highest RMSE were found to be located in the region of the gypsum plates facing the cavity region, in comparison to the other

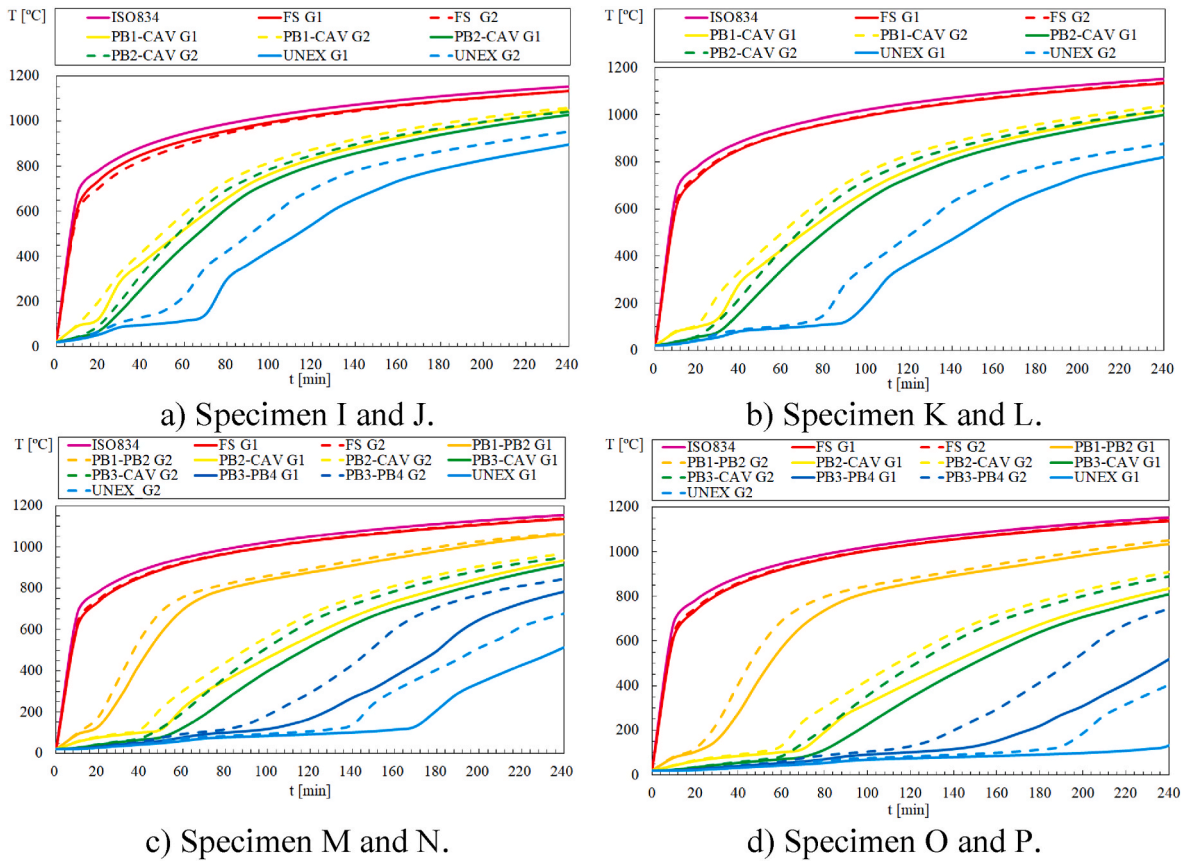

Fig. 16. Temperature evolution during fire exposure using stud type ∑.

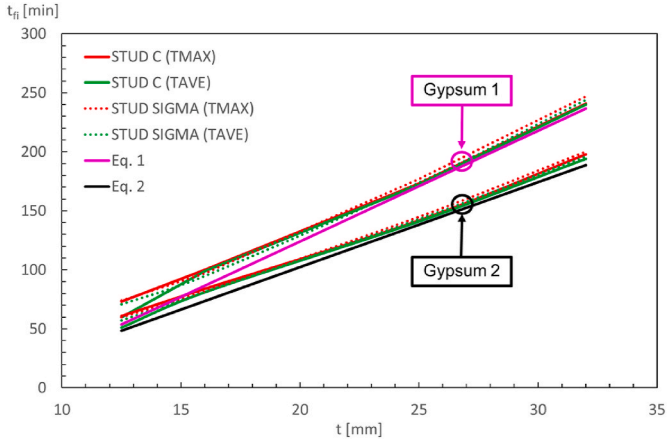

Fig. 17. Insulation fire resistance (t_{fi}) for different gypsum types and layers (thickness = t).

measurements. This error might be explained by the measuring position of the thermocouples. The RMSE also increases with respect to the duration of the test, where singular events occur more frequently, such as ablation, cracks and other heat releases.

Finally, the experimental fire resistance (insulation) can be compared with the numerical results, see Table 5. The experimental fire resistance for insulation was 89 min and is usually determined by the temperature measured on the unexposed surface which can not increase the average temperature above the initial average temperature by more than 140 °C, or increase, at any location, the maximum temperature above the initial average temperature by more than 180 °C [37]. The numerical prediction for the average and the maximum temperature was determined based on the temperature values from 14 nodes (two nodes located on the unexposed side of the gypsum plate on the back side of each stud and four nodes on the unexposed side of the gypsum plate on the back side of the cavity region). Solution method 1 overpredicts this value with a difference of 11%, while solution method 3 underpredicts the fire resistance by 18%.

Specimen 2 is made with double gypsum boards on each side [33]. According to the authors, the inner gypsum boards near the cavity region were attached with small-length self-drilling screws spaced every 300 mm and the second layer of gypsum boards was attached with longer self-drilling screws using the same space between centres. This specimen was submitted to 3 h of fire test, and after all, during the final inspection made by the authors, both gypsum plates PB1 and PB2 (most exposed) were still intact and the studs were in good condition. The furnace temperature decreased after 180 min as depicted in the graph. The temperature of specimen 2 did not rise as quickly as in cavity-insulated specimens since the gypsum board PB2 (fireside in contact with the cavity) was allowed to transfer heat by radiation and convection to the inner side of the cavity. The heat flow across the cavity into PB3 worked as a heat sink to the fireside gypsum plates. The average temperature of surface PB2-CAV is slightly higher than the average temperature of PB3-CAV and the difference was always below 70 °C. The average temperature from the gypsum boards PB3 and PB4 showed a plateau after 100 min. The temperature plateau between these gypsum boards PB3-PB4 was explained by the high degree of integrity of the most exposed gypsum boards (PB1 and PB2). According to Fig. 11, the increase in LSF temperature just started after 60 min. The temperature was under 120 °C at the end of the plateau. This plateau was followed by a gradual temperature rise, reaching 400 °C after 115 min. The experimental fire resistance (criteria I) was defined as greater than 200 (the maximum duration of the fire test).

Fig. 11 presents the difference between the experimental and

numerical results for specimen 2 in terms of the temperature evolution with time as presented in the previous validation. The average temperature (UNEX) is compared for all solution methods. The steel temperature starts to increase later because this specimen presents a double gypsum protection layer. Once again, solution method 2 underpredicts the fire resistance, giving a result of 168 min, which compares with the one obtained experimentally by the authors (>200 min). This method also presents higher temperature values for the steel components (HF, WEB, CF) when compared to the other solution methods, due to the same reason. Solution method 1 predicts 240 min of fire resistance, even though the numerical solution is only presented up to the maximum time from experimental tests. Since the fire test was stopped at 200 min, there is no information on the bulk temperature (cavity temperature), thus the fire resistance from solution method 3 could not be determined, but based on the calculated values it will be higher than 200 min. The maximum velocity decreases with the duration of the fire simulation, after reaching the maximum at 30 min. There is a good correlation between the vector field and the air temperature, which can explain the existence of more recirculating zones in the cavity.

Fig. 12 depicts the temperature field from specimen 2, when using all the three solution methods. The results are presented for 60 min and 120 min after the start of the simulation.

As observed in the previous comparison, solution method 2 is producing a higher RMSE as the component related to the heat flow (convection) is missing and it is responsible to raise the temperature in the cavity region, with higher differences noted in the gypsum layer facing the cavity region. Table 6, Table 7, and Table 8 present the RMSE determined for each solution method. For the first 180 min of comparison, solution method 1 presents an average RMSE of 41.3 °C, while solution method 2 is presenting an average RMSE of 105.1 °C. The RMSE for solution method 3 is presenting an average RMSE of 37.5 [a]C.

The highest RMSE were found to be located in the region of the gypsum plates facing the cavity region or located in the region between the gypsum boards, in comparison with the respective measurements. This can be justified by the uncertainty in the experimental measurement facing the cavity region and the possible existence of a gap between both gypsum boards (not allowing for perfect contact as assumed in the numerical model), respectively. The RMSE also increases with the duration of the fire test, where singular events are expected. The experimental fire resistance can be compared with the numerical results in Table 9. The experimental test was terminated before reaching the fire resistance criterion (200 min).

Finally, the test Specimen 3 is considered herein for the sake of comparison. This specimen was built with two gypsum boards. Both tracks had bigger lengths when compared to the distance between the studs. This extension has been covered with additional 100 mm wide gypsum [6]. The average temperature profile for specimen 3 is presented in Fig. 13. The FS thermocouple follows a monotonous growth until 210 min. After that, FS shows a temperature drop, with a sudden increase in PB1-PB2. According to Dias et al. [6], this event is justified by the sudden fall-off of the gypsum board PB1. The unexposed surface temperature (UNEX) development was quite uniform over the surface, when comparing the copper disk thermocouples applied on this surface. The insulation failure was defined by the average temperature criterion after 252 min of fire exposure. The steel temperature history also displayed a similar history, where after an initial plateau, the LSF temperature gradually rise up to 220 min. But after 220 min, both the HF and CF temperatures rose rapidly again. This behaviour was justified by the sudden fall-off in the fireside external gypsum layer. The average temperature (UNEX) is compared for all solution methods. This specimen has almost the same level of fire protection when compared to specimen 2, which means that for the same wall thickness, the geometry effect of the stud is not affecting the insulation fire resistance. Specimen 3 has a difference in the fire resistance of 1.6% and 0.6% with respect to specimen 2, when comparing solution method 1 and solution method 2, respectively.

For solution method 3, the comparison is not possible due to the inexistence of bulk temperature values after 200 min in specimen 2. As before, solution method 2 underpredicts the fire resistance (169 min). This solution method also presents higher temperature values for the steel components (HF, WEB, CF) when compared to the other solution methods. Solution method 1 predicts 244 min of fire resistance. The insulation fire resistance from solution method 3 presents an intermediate value of 225 min. The maximum velocity decreases with the duration of the fire simulation, after reaching the maximum at 30 min.

Fig. 14 depicts the temperature field from specimen 3. The results are presented for the same time of the previous specimen, 60 min and 120 min after the start of the simulation. These temperature fields are very similar to the ones obtained for the specimen 2.

Once more, solution method 2 is producing the highest RMSE, as the convection heat flux is missing. This missing heat flux is responsible to raise the temperature in the cavity region, with higher differences noted in the material in contact with the cavity region. Table 10, Table 11, and Table 12 present the RMSE determined for each solution method. For the first 180 min of comparison, solution method 1 presents an average RMSE of 39.2 °C, while solution method 2 is presenting an average RMSE of 74.4 °C. The RMSE for solution method 3 is presenting an average RMSE of 41 °C.

The highest RMSE were found to be located in the region of the gypsum boards facing the cavity region or located in the region between the gypsum plates, in comparison to the other measurements. This can be justified by the different singularities in the behaviour of the materials in the experiments and in the numerical simulation, which assumes perfect contact between the materials. The RMSE also increases with respect to the end of the test, where other singular events are expected, as mentioned before. The experimental fire resistance is compared with the numerical results in Table 13. Both solution methods 1 and 3 present small relative errors, representing 3 and 10%, while solution method 2 presents the highest relative error (33%).

4. Parametric study

This parametric study presents the effect of the gypsum type, the effect of the number and the thickness of the gypsum boards in the fire resistance of different internal LSF walls. Both stud geometries have been used for this parametric study when submitted to standard fire (ISO834 and AS1530.4). The LSF structure was made with three studs ("C" or "Σ"), using two different gypsum boards (denoted Gypsum 1 or Gypsum 2) and a variable number of gypsum plates (1 or 2) and thicknesses (12.5 or 16 mm). The thermal properties are defined in Fig. 8. The total number of simulations was 16. Solution method 1 has been used to predict the fire resistance, see Table 14.

Fig. 15 presents the temperature evolution in the gypsum parts of the LSF walls when using "C" stud type. Higher fire resistance is expected when using gypsum 1, see UNEX evolution. This increase in fire resistance depends on the number and thickness of protection layers.

It should be noted that, with the increase in thickness and in the number of gypsum layers, the temperature in the unexposed surface (UNEX) decreases. This occurs for both gypsum types, but gypsum 1 presents better fire performance. Fig. 16 presents the same comparison but using the stud type Σ in the LSF. Similar conclusions can be presented and no significative differences were found.

With these simulations, one was able to define the insulation fire resistance for all simulations. Fig. 17 presents the average and maximum temperature criteria for all the specimens. Good correlation was found between the fire resistance and the thickness of the protection gypsum boards.

Based on these results, a new proposal is presented to determine the insulation fire resistance as a function of the thickness of the gypsum boards. These two equations are only valid for these gypsum types and for the equivalent thickness of the gypsum plates. Eq. (1) is valid for gypsum type 1, while Eq. (2) is only valid for gypsum type 2. These

equations have been determined with a safety level determined by the average values minus two times the value of the standard deviation. The regression coefficients R^2 were determined to be 0.99 for both gypsum types, which means that predictions approximate very well the real data points.

$$t_{fi} = 9.8 \times t - 63.7 \ (12.5 \leq t \leq 32) \quad (1)$$

$$t_{fi} = 7.3 \times t - 41.6 \ (12.5 \leq t \leq 32) \quad (2)$$

5. Conclusions

This study presents a comparison between three different numerical modelling techniques to calculate the fire resistance (insulation) of LSF partition walls, namely using the Computational Fluid Dynamics with Finite Volume Method (FVM), the Finite Element Method (FEM) and a hybrid technique combining experimental temperatures and FEM (denoted H-FEM). The simulations are using the 2D cross section modelling of non load bearing walls and results may differ from 3D results, due to the existence of connections, joints and other mechanical systems. The solution method 1 should be the one that can enforce major differences due to the existence of a higher volume of the cavity region, when compared with the density-driven forces produced by the higher temperature gradients in the vertical direction of the LSF walls. Solution methods 2 and 3 are also affected by the dimension of the analysis, mainly when tracks or noggins are used in the LSF wall.

All the computational models are overpredicting the experimental temperatures because standard furnace temperatures were used (not real furnace temperatures). On the other hand, some fire events are missing in simulations from solution methods 1 and 2 (cracks, fall off of gypsum plates), which can anticipate temperature growth. The effective properties are used to mimic these experimental fire events, but may be insufficient to fit the model. The boundary conditions are following the standards for the exposed and unexposed sides, but no information is given for the cavity region.

Nevertheless, solution methods 1 (CFD simulation with FVM) and 3 (hybrid model simulation with FEM) provide the smaller RMSE during the simulation of the experimental tests. The performance was determined by the comparison of numerical and experimental results for a time step of 10 min. Solution method 2 overpredicts the temperatures in the cavity region (gypsum boards and LSF) due to the inexistence of the convective heat flux. Solution method 3 requires the information about the bulk temperature of the cavity region. This information van be retrieved from previous experimental tests, and depends mainly on the number, thickness and type of the gypsum plates. The cladding system is typically made using a finite number of gypsum plates and can be used to establish typical bulk temperature in the cavity region.

The fire resistance (insulation) was also predicted using these three solution methods. The relative error is also smaller for solution methods 1 and 3, when compared to the experimentally obtained one. This might be explained by the same reason aforementioned.

Based on the results of the parametric study, one can conclude that the shape of the stud does not play an important contribution to the fire resistance (insulation), when keeping the same LSF wall thickness. The type of gypsum board can change the fire resistance (insulation) of the LSF wall, with the boards of Gypsum type 1 presenting higher fire resistance (insulation) when compared to Gypsum 2, being the difference greater when the thickness of the plates increases.

Finally, a new proposal was presented to determine the fire resistance (insulation). This proposal can be used to calculate the ability of the LSF partition walls to sustain the temperature on the unexposed side.

Declaration of competing interest

The authors declare that they have no known competing financial interests or personal relationships that could have appeared to influence the work reported in this paper.

Data availability

Data will be made available on request.

References

[1] Y. Sakumoto, T. Hirakawa, H. Masuda, K. Nakamura, Fire resistance of walls and floors using light-gauge steel shapes, J. Struct. Eng. 129 (November) (2003) 1522–1530, https://doi.org/10.1061/(ASCE)0733-9445(2003)129:11(1522).

[2] P.N. Kolarkar, Structural and Thermal Performance of Cold-Formed Steel Stud Wall Systems under Fire Conditions, Queensland University of Technology, 2010.

[3] D. Lázaro, E. Puente, M. Lázaro, P.G. Lázaro, J. Peña, Thermal modelling of gypsum plasterboard assemblies exposed to standard fire tests, Fire Mater. 40 (4) (2016) 568–585, https://doi.org/10.1002/fam.2311.

[4] A.D. Ariyanayagam, M. Mahendran, Fire tests of non-load bearing light gauge steel frame walls lined with calcium silicate boards and gypsum plasterboards, Thin-Walled Struct. 115 (January) (Jun. 2017) 86–99, https://doi.org/10.1016/j.tws.2017.02.005.

[5] Y. Dias, M. Mahendran, K. Poologanathan, Full-scale fire resistance tests of steel and plasterboard sheathed web-stiffened stud walls, Thin-Walled Struct. 137 (January) (2019) 81–93, https://doi.org/10.1016/j.tws.2018.12.027.

[6] Y. Dias, P. Keerthan, M. Mahendran, Fire performance of steel and plasterboard sheathed non-load bearing LSF walls, Fire Saf. J. 103 (October 2018) (2019) 1–18, https://doi.org/10.1016/j.firesaf.2018.11.005.

[7] H. Magaraboosanam, A. Ariyanayagam, M. Mahendran, Fire resistance of non-load bearing LSF walls with varying cavity depth, Thin-Walled Struct. 150 (October 2019) (2020), https://doi.org/10.1016/j.tws.2020.106675.

[8] Y. Tao, M. Mahendran, Fire tests and thermal analyses of LSF walls insulated with silica aerogel fibreglass blanket, Fire Saf. J. 122 (April) (2021), 103352, https://doi.org/10.1016/j.firesaf.2021.103352.

[9] S. Gnanachelvam, A. Ariyanayagam, M. Mahendran, Effects of insulation materials and their location on the fire resistance of LSF walls, J. Build. Eng. 44 (May) (2021), https://doi.org/10.1016/j.jobe.2021.103323.

[10] M.A. Sultan, A model for predicting heat transfer through noninsulated unloaded steel-stud gypsum board wall assemblies exposed to fire, Fire Technol. 32 (3) (1996) 239–259, https://doi.org/10.1007/BF01040217.

[11] G. Thomas, Thermal properties of gypsum plasterboard at high temperatures, Fire Mater. 26 (1) (2002) 37–45, https://doi.org/10.1002/fam.786.

[12] C.N. Ang, Y.C. Wang, The effect of water movement on specific heat of gypsum plasterboard in heat transfer analysis under natural fire exposure, Construct. Build. Mater. 18 (7) (2004) 505–515, https://doi.org/10.1016/j.conbuildmat.2004.04.003.

[13] P. Keerthan, M. Mahendran, Numerical studies of gypsum plasterboard panels under standard fire conditions, Fire Saf. J. 53 (2012) 105–119, https://doi.org/10.1016/j.firesaf.2012.06.007.

[14] P. Keerthan, M. Mahendran, Thermal performance of composite panels under fire conditions using numerical studies: plasterboards, rockwool, glass fibre and cellulose insulations, Fire Technol. 49 (2) (2013) 329–356, https://doi.org/10.1007/s10694-012-0269-6.

[15] S. Gunalan, M. Mahendran, Finite element modelling of load bearing cold-formed steel wall systems under fire conditions, Eng. Struct. 56 (2013) 1007–1027, https://doi.org/10.1016/j.engstruct.2013.06.022.

[16] M. Rusthi, Keerthan Mohamed, Ariyanayagam Poologanathan, Deloge Anthony, Mahendran, Numerical studies of gypsum plasterboard and MGO board lined LSF walls exposed to fire, in: Proceedings of PLSE 2015, 2015, pp. 1077–1084.

[17] Jonathan Vallée, Reliability of Fire Barriers, Lund University - Faculty of Engineering Department, 2016.

[18] Y. Tao, M. Mahendran, A. Ariyanayagam, Numerical study of LSF walls made of cold-formed steel hollow section studs in fire, Thin-Walled Struct. 167 (July) (2021) 108181, https://doi.org/10.1016/j.tws.2021.108181.

[19] P. Samiee, S. Esmaeili Niari, E. Ghandi, Thermal and structural behavior of cold-formed steel frame wall under fire condition, Eng. Struct. 252 (October 2021) (2022) 113563, https://doi.org/10.1016/j.engstruct.2021.113563.

[20] I.R. Upasiri, K.M.C. Konthesigha, S. Nanayakkara, K. Poologanathan, P. Gatheeshgar, D. Perera, Fire performance of lightweight concrete-filled LSF wall panels, Structures 40 (October 2021) (2022) 1039–1055, https://doi.org/10.1016/j.istruc.2022.04.081.

[21] CEN, EN 1991-1-2, Eurocode 1: Actions on Structures – Part 1-2: General Actions – Actions on Structures Exposed to Fire vol. 59, CEN- European Committee for Standardization. CEN- European Committee for Standardization, Brussels, 2002.

[22] D. Perera, et al., Novel conventional and modular LSF wall panels with improved fire performance, J. Build. Eng. 46 (May 2021) (2022) 103612, https://doi.org/10.1016/j.jobe.2021.103612.

[23] P.A.G. Piloto, M.S. Khetata, A.B.R. Gavilán, Fire performance of non-loadbearing light steel framing walls - numerical simulation, in: 7th International Conference Mechanics and Materials in Design, 2017, pp. 1603–1610.

[24] M. Khetata, L. Fernandes, C. Marinho, P. Piloto, A. Gavilán, H. Razuk, Fire resistance of non-loadbearing light steelframing walls: numerical validation, in: XI Portuguese Congress on Steel and Composite Construction, CMM 2017, 2017, pp. 853–862.

[25] P.A.G. Piloto, M.S. Khetata, A.B.R. Gavilán, Fire performance of non-loadbearing light steel framing walls-numerical and simple calculation methods, MATTER Int.

J. Sci. Technol. 3 (3) (2017) 13–23, https://doi.org/10.20319/mijst.2017.33.1323FIRE.
[26] P.A.G. Piloto, Fire resistance of cold-formed steel walls with composite panels : results from insulation rating (I) and loadbearing prediction rating (R), Metálica international, no. 7, Portuguese Association for Steel and Composite Construction, Coimbra (2018) 12–17.
[27] P.A.G. Piloto, M.S. Khetata, A.B.R. Gavilán, Loadbearıng capacıty of LSF walls under fıre exposure, MATTER Int. J. Sci. Technol. 4 (3) (2018) 104–124, https://doi.org/10.20319/mijst.2018.43.104124.
[28] S.M. Khetata, P.A.G. Piloto, A.B.R. Gavilán, Fire resistance of composite non-load bearing light steel framing walls, J. Fire Sci. 38 (2) (Mar. 2020) 136–155, https://doi.org/10.1177/0734904119900931.
[29] M.H. Alves, G. Constantini, A. Ianni, E.F.A. Kimura, A. Meda, P.A.G. Piloto, Fire performance of non-load-bearing double-stud light steel frame walls: experimental tests, numerical simulation, and simplified method, Fire Mater. (2021), https://doi.org/10.1002/fam.2969. February, p. fam.2969.
[30] P.A.G. Piloto, M.S. Khetata, A.B. Ramos-Gavilán, Analysis of the critical temperature on load bearing LSF walls under fire, Eng. Struct. 270 (July) (2022) 114858, https://doi.org/10.1016/j.engstruct.2022.114858.
[31] ANSYS 2023 R1, in: ANSYS Fluent Theory Guide, vol. 15317, ANSYS Inc., USA, 2013, p. 814, no. November.
[32] ANSYS 2023 R1, ANSYS Parametric Design Language Guide 15317 (October) (2012) 724–746.
[33] P. Kolarkar, M. Mahendran, Experimental studies of non-load bearing steel wall systems under fire conditions, Fire Saf. J. 53 (Oct. 2012) 85–104, https://doi.org/10.1016/j.firesaf.2012.06.009.
[34] CEN, EN 1993-1-2: Design of Steel Structures - Part 1-2: General Rules - Structural Fire Design, CEN - European Committee for Standardization, Brussels, 2005.
[35] CEN, Pr EN 1995-1.2, Eurocode 5: Design of Timber Structures - Part 1-2: General - Structural Fire Design, CEN - European Committee for Standardization, Brussels, 2020.
[36] Y.A. Çengel, A.J. Ghajar, Heat and Mass Transfer: Fundamentals and Applications, fifth ed., McGraw-Hill Education, New York, 2015.
[37] CEN, in: EN 1363-1: Fire Resistance Tests Part 1 : General Requirements, CEN-European Committee for Standardization, Brussels, 2020, p. 52.